



CHROMOSPHERICALLY ACTIVE STARS IN THE RAVE SURVEY. II. YOUNG DWARFS IN THE SOLAR NEIGHBORHOOD

M. ŽERJAL¹, T. ZWITTER¹, G. MATIJEVIĆ², E. K. GREBEL³, G. KORDOPATIS², U. MUNARI⁴, G. SEABROKE⁵, M. STEINMETZ², J. WOJNO², O. BIENAYMÉ⁶, J. BLAND-HAWTHORN⁷, C. CONRAD², K. C. FREEMAN⁸, B. K. GIBSON⁹, G. GILMORE¹⁰, A. KUNDER², J. NAVARRO^{11,19}, Q. A. PARKER^{12,13}, W. REID^{14,15}, A. SIVIERO¹⁶, F. G. WATSON¹⁷, AND R. F. G. WYSE¹⁸

¹ Faculty of Mathematics and Physics, University of Ljubljana, Jadranska 19, 1000 Ljubljana, Slovenia; marusa.zerjal@fmf.uni-lj.si

² Leibniz-Institut für Astrophysik Potsdam (AIP), An der Sternwarte 16, D-14482, Potsdam, Germany

³ Astronomisches Rechen-Institut, Zentrum für Astronomie der Universität Heidelberg, Mönchhofstr. 12-14, D-69120 Heidelberg, Germany

⁴ INAF Osservatorio Astronomico di Padova, I-36012 Asiago, Italy

⁵ Mullard Space Science Laboratory, University College London, Holmbury St Mary, Dorking, RH5 6NT, UK

⁶ Observatoire astronomique de Strasbourg, Université de Strasbourg, CNRS, UMR 7550, 11 rue de l'Université, F-67000 Strasbourg, France

⁷ Sydney Institute for Astronomy, School of Physics, University of Sydney, NSW 2006, Australia

⁸ Research School of Astronomy and Astrophysics, Australia National University, Weston Creek, Canberra, ACT 2611, Australia

⁹ E.A. Milne Centre for Astrophysics, University of Hull, Hull, HU6 7RX, UK

¹⁰ Institute of Astronomy, University of Cambridge, Madingley Road, Cambridge CB3 0HA, UK

¹¹ University of Victoria, Victoria, BC, V8P 5C2, Canada

¹² Department of Physics, The University of Hong Kong, Hong Kong SAR, China

¹³ Laboratory for Space Research, The University of Hong Kong, Hong Kong SAR, China

¹⁴ Department of Physics and Astronomy, Macquarie University, Sydney, NSW 2109, Australia

¹⁵ Western Sydney University, Locked Bag 1797, Penrith South DC, NSW 1797, Australia

¹⁶ Dipartimento di Fisica e Astronomia Galileo Galilei, Università di Padova, Vicolo dell'Osservatorio 3, I-35122 Padova, Italy

¹⁷ Australian Astronomical Observatory, P.O. Box 915, North Ryde, NSW 1670, Australia

¹⁸ Johns Hopkins University, Homewood Campus, 3400 N Charles Street, Baltimore, MD 21218, USA

Received 2016 August 14; revised 2016 November 8; accepted 2016 November 22; published 2017 January 18

ABSTRACT

A large sample of over 38,000 chromospherically active candidate solar-like stars and cooler dwarfs from the RAVE survey is addressed in this paper. An improved activity identification with respect to the previous study was introduced to build a catalog of field stars in the solar neighborhood with an excess emission flux in the calcium infrared triplet wavelength region. The central result of this work is the calibration of the age–activity relation for main-sequence dwarfs in a range from a few 10 Myr up to a few Gyr. It enabled an order of magnitude age estimation of the entire active sample. Almost 15,000 stars are shown to be younger than 1 Gyr and ~ 2000 younger than 100 Myr. The young age of the most active stars is confirmed by their position off the main sequence in the $J - K$ versus $N_{UV} - V$ diagram showing strong ultraviolet excess, mid-infrared excess in the $J - K$ versus $W_1 - W_2$ diagram, and very cool temperatures ($J - K > 0.7$). They overlap with the reference pre-main-sequence RAVE stars often displaying X-ray emission. The activity level increasing with the color reveals their different nature from the solar-like stars and probably represents an underlying dynamo-generating magnetic fields in cool stars. Of the RAVE objects from DR5, 50% are found in the TGAS catalog and supplemented with accurate parallaxes and proper motions by *Gaia*. This makes the database of a large number of young stars in a combination with RAVE's radial velocities directly useful as a tracer of the very recent large-scale star formation history in the solar neighborhood. The data are available online in the VizieR database.

Key words: catalogs – stars: activity – stars: chromospheres – stars: emission-line, Be – stars: evolution – stars: pre-main sequence

1. INTRODUCTION

A large portion of solar-like and later-type dwarf stars exhibit signs of chromospheric activity during their young ages, especially before they reach solar age (Mamajek & Hillenbrand 2008, hereafter M08). Chromospheric activity develops in stars with a subsurface convective layer, i.e., stars in the cooler part of the Hertzsprung–Russell diagram. There are two components responsible for the excessive emission flux. The dominant component is produced by a complex rotation-driven magnetic dynamo. It is superimposed on the basal emission (e.g., Schrijver et al. 1989) originating from the acoustic energy released into the atmosphere from the ubiquitous convective cells. While the basal emission remains constant, the loss of the angular momentum of the star over

time leads to the decline of the rotation period and activity. Because the decline of the excess flux over hundreds of millions of years exceeds the short-term variations on the scales of days (stellar flares), months (starspot rotation), and decades (solar 11 year cycle analogues)—e.g., Wright et al. (2004)—this observable is a suitable age estimator. While precise dating is not possible for many reasons (e.g., pre-main-sequence and zero-age main-sequence stars exhibit a broad range of activity levels at a given age; Soderblom 2010), an order of magnitude age estimate is easily attainable in the range from a few tens of millions of years up to a few Gyr.

In contrast to the more fundamental but observationally demanding gyrochronology-based dating, the detection of chromospheric activity is straightforward as it manifests itself in a wide range of emission intensities in the strongest spectral lines ($H\alpha$; $H\beta$; Ca II H&K; Ca II infrared triplet; Mg II h&k—the latter are not visible from the ground). A single spectral

¹⁹ Senior CIFAR Fellow.

measurement with moderate signal-to-noise ratio (>20 per pixel) and mid-range resolving power is adequate for stellar age estimation using the age–activity relation. This fact is of huge importance in the era of large Milky Way spectroscopic surveys covering hundreds of thousands of stars as it enables the age estimation of a large number of young candidates. Such catalogs of young stars enhanced with the individual abundances (e.g., the Galah (De Silva et al. 2015) and *Gaia*-ESO (Smiljanic et al. 2014) Surveys) and astrometric data and parallaxes from *Gaia* (Michalik et al. 2015) hold a huge potential for the investigation not only of the recent star formation history in the solar neighborhood and the evolution of the Milky Way galaxy but the nature of stellar dynamo mechanisms and the influence of stellar activity and abundances on the planetary environments as well.

In this paper we investigate the data from the RAVE Survey (RAial Velocity Experiment,²⁰ Steinmetz et al. 2006; Zwitter et al. 2008; Siebert et al. 2011; Kordopatis et al. 2013; Kunder et al. 2016). While most of the literature studying chromospheric activity covers the strong Ca II H&K (3967 and 3933 Å; Zhao et al. 2015 for example report on a catalog of 120,000 F, G, and K stars with Ca II H&K emission in the first LAMOST data release), RAVE focuses on the Ca II infrared triplet (Ca II IRT; 8498, 8542 and 8662 Å). The latest data release (DR5, Kunder et al. 2016) includes 520,781 multi-fiber spectroscopic measurements of 457,588 stars collected between 2003 and 2013 with radial velocity determination being one of the main goals of the survey.

With the help of an efficient unsupervised stellar classification algorithm based on normalized stellar fluxes and independent of stellar parameters (locally linear embedding, LLE; Matijević et al. 2012, hereafter M12) tens of thousands of candidate active stars have been uncovered. A large catalog of 44,000 candidate chromospherically active RAVE stars described in the first paper in the series (Žerjal et al. 2013, hereafter Z13) contains over 14,000 stars above the 2σ excess emission detection limit.

Around 65% of all the objects in the RAVE database (and 60% of the active candidates) are also found in the Tycho-2 astrometric catalog (Høg et al. 2000). Because these dwarfs reside in the solar neighborhood, their distance errors in the first *Gaia* data release (TGAS; “using the positions from the Tycho-2 Catalog as additional information for a joint solution with early *Gaia* data”; Michalik et al. 2015) are expected to be of the order of 10%, a number that will become considerably more precise with future data releases (reaching a level of $\sim 1\%$; e.g., Bailer-Jones et al. 2013). The catalog of active stars in combination with radial velocities (provided by RAVE) and reliable distances and proper motions will directly enable the study of the early stellar evolution and recent star formation history in the local neighborhood.

The data set will be significantly enhanced by the *Gaia*-RVS catalog (Radial Velocity Spectrometer, covering the same Ca II IRT domain, Katz et al. 2004; Cropper & Katz 2011). By the end of the mission, the set of around nine million stars (with their G_{RVS} magnitude brighter than ~ 11.75 and the signal-to-noise ratio of their spectra over 20 per pixel) will be the largest database in which to look for active stars.

In Paper I (Z13) we listed our selection of candidate active stars, in the present paper II we derive their ages. First, we

introduce an improved activity identification procedure by eliminating stars with nonchromospheric sources of emission from the original catalog (Section 2). The catalog is enhanced with 46 additional very active candidates not included in Z13. A study of the $J - K$ versus $N_{UV} - V$ diagram in Section 3 shows an offset of the youngest stars with the highest emission levels from the main sequence. This group of stars accumulates in a relatively confined part of the plot where young, T Tauri, pre-main-sequence stars and stars with X-ray emission are found. A calibration of the age–activity relation using ages from the literature is presented in Section 4 as the leading result of this paper which allows an order of magnitude age determination for more than 22,000 young RAVE stars in the solar neighborhood. The lower and upper distance limit determinations are described in Section 5. Conclusions with a discussion, open questions, and future plans, including orbital simulations of the youngest stars using *Gaia* astrometry, are presented in Section 6. A table of the external reference ages used in the age–activity relation calibration is presented in the Appendix.

2. IMPROVED CATALOG

The catalog of candidate active stars used in this work is described in detail by Z13. Here we very briefly review the determination of activity levels and basic characteristics of the sample to allow the reader to better understand the context of present study.

Chromospheric activity in the RAVE domain manifests itself in an excessive emission flux in the Ca II IRT while the rest of the spectrum remains indistinguishable from an inactive state. The strength of the emission can range from marginally detectable levels to individual cases with fluxes above the continuum level. The qualitative classification of the RAVE database using the LLE technique (M12) based entirely on normalized spectra revealed over 44,000 stars with the possible presence of an excessive emission in the Ca II IRT. For the detailed selection criteria, see Z13.

The photospheric component of the flux was eliminated from the active candidate star by the subtraction of the best-matching inactive template spectrum. For the purpose of the spectral subtraction technique, a database of over 12,000 inactive single solar-like or later-type main-sequence dwarfs with no emission or any other peculiarities was built from the measured RAVE sample. Although chromospheric activity has been detected in evolved stars (e.g., Wilson 1976), objects with $\log g < 3.5$ were excluded from the inactive sample because magnetic activity is not expected to be notably present in giant stars above the main sequence. Rutten (1984, hereafter R84) showed that the emission rate in evolved stars is very close to the basal level.

The number of stars in the inactive set is sufficient to cover the entire parameter space of active candidates, including the effective temperature, gravity and metallicity, varied noise realizations, and possible variations of resolving power along the spectra. Most of the inactive stars are concentrated around the solar temperature. It becomes less likely to find an inactive star in the cooler regions of the main sequence because active stars become more and more dominant there. Due to lack of inactive stars above the main sequence, the same database of 12,000 stars is used for the activity estimation of the pre-main-sequence stars.

²⁰ <https://www.rave-survey.org/>

The advantage of the approach using the measured inactive library from the RAVE Survey in contrast to a synthetic data set is the fact that active and inactive sets share the same instrumental profile of the spectra (e.g., resolving power and point-spread function along the spectra). It avoids problems with an invalid assumption of the local thermodynamic equilibrium in the chromospheric layer used in models which affects the cores of the strongest lines that are at the same time sensitive to magnetic activity. Moreover, the determination of the best-matching templates is parameter-free because it is based solely on the comparison of the normalized fluxes of active and inactive spectra. Atmospheric parameters are excluded from the template search. This is an important aspect as values for the highly active stars, together with the radial velocities, could be inaccurate due to the influence of the excessive flux. Additionally, the parameter estimation for RAVE stars with temperature cooler than 4000 K shows systematic offsets. The search for the best-matching template by comparing normalized fluxes was performed in an iterative algorithm to apply radial velocity corrections. To avoid the impact of the shallower calcium lines, these regions were eliminated across a range of $\pm 2.5 \text{ \AA}$ from the line cores of all active and template spectra. Equivalent widths of the excessive emission for each calcium line in the spectrum combined into the sum $EW_{\text{IRT}} = EW_{8498} + EW_{8542} + EW_{8662}$ are used as the activity proxy.

For reference, activity of the inactive database was estimated using the same method. The distribution of equivalent widths in the latter case is centered at -0.05 \AA with a standard deviation of $\sigma = 0.16 \text{ \AA}$. An investigation of the subtracted spectra revealed that their average value outside calcium lies slightly below zero ($\sim 10^{-3}$ in the normalized flux units), which translates to the negative offset of the emission equivalent width. σ is accepted as an internal error on the derived EW_{IRT} .

Another contribution to the uncertainty is the intrinsic time variability of the activity on the scales of days (stellar flares), months (starspot rotation), and decades (solar 11 year cycle analogues). The statistics of the repeated observations of the same active stars from the active RAVE catalog (1146 stars, of which 30% were observed more than twice) shows that the median difference between the minimum and maximum values of activity for a single star ($EW_{\text{IRT}}^{\text{max}} - EW_{\text{IRT}}^{\text{min}}$) is 0.15 \AA (Figure 1, panel (a)). In general more active stars show higher variability rates (Radick et al. 1998). A moving average of $EW_{\text{IRT}}^{\text{max}} - EW_{\text{IRT}}^{\text{min}}$ versus $EW_{\text{IRT}}^{\text{max}}$ confirms the statement (panel (b)). For stars with $EW_{\text{IRT}}^{\text{max}}$ between 1 and 3 \AA , the mean variability is 0.33 \AA (panel (c)). It is important to stress that intrinsic variations of the chromospheric activity occur on timescales of days to months, to tens of years (due to flares, stellar rotation of active regions and spots, and 11 year solar cycle analogues). The variations are smaller than the global decline of the activity with time.

2.1. The Aquarius Overdensity

The Aquarius stream, which is known to consist of at least 15 stars between $30^\circ < l < 75^\circ$ and $-70^\circ < b < -50^\circ$, has been identified in the RAVE data by Williams et al. (2011). The stream members are giants at distances of 0.5–10 kpc with radial velocities $\sim -200 \text{ km s}^{-1}$ and estimated to be 10 Gyr old. An additional group of 11 adjacent fields of red stars with $J - K > 0.7$ was intentionally observed by RAVE in the direction of the Aquarius constellation at $35^\circ < l < 75^\circ$ and

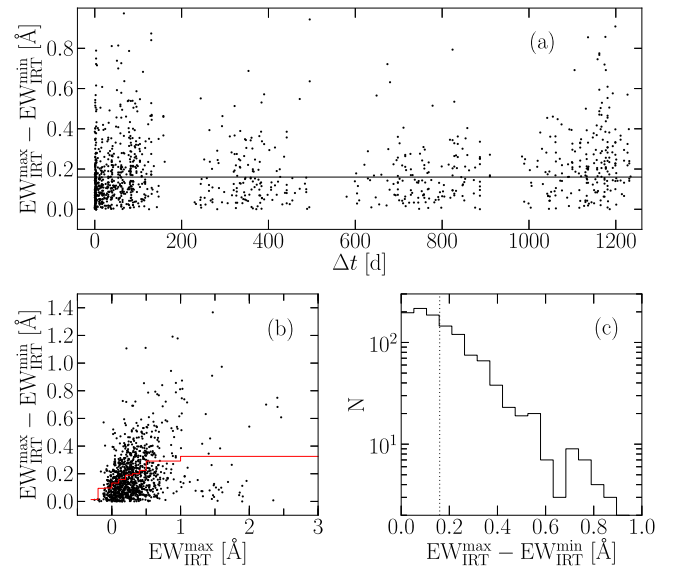


Figure 1. Time variability of the Ca II IRT chromospheric emission for stars with multiple measurements measured as the difference between the maximal and minimal activity rate. Activity detection limit (0.16 \AA) is shown with the black line. The majority of stars in the plot have two repeated observations; Δt is the time difference between the measurements. More active stars exhibit higher variability rates (panel (b)); the moving average is shown with the red line: bin size between -0.5 and 0.5 \AA is 0.1 \AA and larger above 0.5 \AA . The median variability of the sample (0.15 \AA) is comparable with the activity detection limit (c).

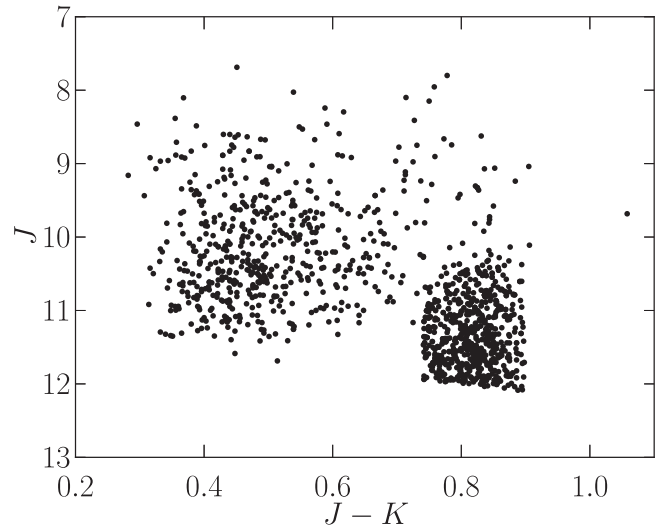


Figure 2. Color-magnitude diagram for Aquarius fields with an overdensity of red stars. J is an apparent magnitude. More red stars were observed to gather more potential Aquarius stream members. Only active candidates are plotted.

$-62^\circ < l < -50^\circ$ in order to collect more stream candidates. As a consequence, a supplementary set of red dwarfs was observed as well. As the probability for activity increases toward the lower part of the main sequence, many of them turned out to be active (Figure 2). Nevertheless, the number of all observed stars in Aquarius and the number of all dwarfs with $\log g > 3.75$, proper motions, and radial velocities show no other peculiarities with respect to similar regions at the same Galactic latitude.

The ratio between red ($J - K \geq 0.7$) active stars and all red RAVE dwarfs in Aquarius is at least 80%. The same is true for stars with $EW_{\text{IRT}} \geq 1 \text{ \AA}$. For this reason the Aquarius fields

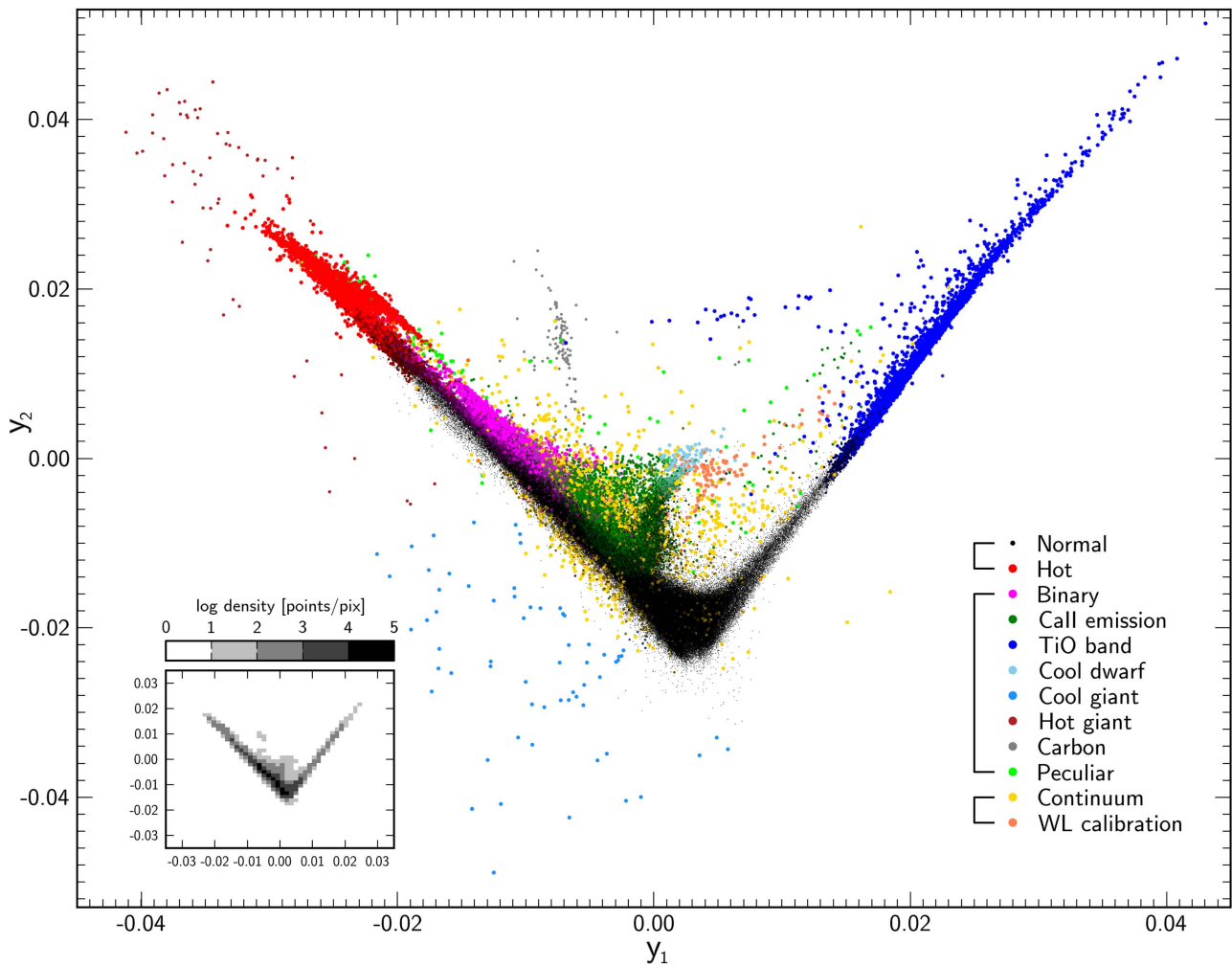


Figure 3. First two dimensions y_1 and y_2 of the projection map of the LLE classification technique that conserves relations between the neighboring points of the high-dimensional manifold. A selected spectrum in the projected space is surrounded by its neighbors from the high-dimensional space. Different colors indicate 11 distinct classes of spectra. Stars showing no peculiarities (“Normal stars” in the plot) are intentionally represented with smaller symbols for clarity. The inset shows the log density of points on the main diagram. Figure adapted from Matijević et al. (2012).

notably contribute to the statistics of the reddest active stars, which are otherwise underpopulated in the RAVE sample due to their low luminosities.

2.2. Improved Activity Identification

The selection of candidates in the catalog is based on the set of morphological flags produced by the spectral classification technique. The classification algorithm compares the flux of the spectrum in question with fluxes from the reference database. The reference database was set up in the process involving an LLE. LLE is a general-dimensionality reduction procedure that conserves relations between the neighboring points of the high-dimensional manifold. Because a selected spectrum in the projected space is surrounded by its neighbors from high-dimensional space, the algorithm is useful for classification purposes. An example of the projection of the RAVE data in two-dimensional space is shown in Figure 3 where different colors indicate 11 distinct classes of spectra.

The method includes three steps. After the nearest neighbors are found for each data point in the original space, the set of weights that best describes the data point as a linear combination of its neighbors is derived. The final, key step is a projection on the low-dimensional space where each point is

still best represented by the same weights from the previous step. For details about the key steps, see M12 or Roweis & Saul (2000), Vanderplas & Connolly (2009), and references therein.

The classification of the RAVE data was broken down into two crucial steps. First, a reference database of the most representative ~ 5000 spectra was established by iteratively sifting the most dense areas of the LLE projection containing the most populated groups of stars. This way all distinct classes of objects were represented as evenly as possible in the final data set. The reference set was then manually assigned classification flags of 11 distinct morphological classes. The classification of the rest of the RAVE spectra was calculated in the second step by comparing the spectra to the reference set. The outcome for each spectrum is a list of 20 flags ordered by the distance between the flux and its nearest reference neighbors. For more details see M12.

A star was selected as an active candidate when at least one nearest neighbor within its first six neighbors from the LLE reference database showed an emission-type spectrum. While this relatively loose criterion helps to unravel marginally active spectra, it on the other hand contaminates the catalog with individual peculiar stars (where some of their nearest neighbors show unsuitable morphology, e.g., binaries, giants, etc.). The

aim of an improved activity identification is thus the elimination of active candidates that show peculiarity other than an excess emission in the Ca II IRT.

The search for such stars was performed in a few independent ways, including nearest neighbor investigation, morphology notes and spectral types from the Simbad database, and visual spectral inspection of the most active stars with manual elimination besides manual exclusion of stars with inadequate atmospheric parameters. Each star was examined using all these criteria.

The largest group of suspicious active candidates was giants with $\log g < 3.7$ (6147 stars). Such stars were excluded from the candidate list introduced in Z13.

An additional 68 hot stars with Paschen lines and shallow calcium lines mistaken for activity were recognized manually. If any of the repeated observations (where available) were recognized as binary all spectra of such objects were removed (101 spectra).

Spectra with $EW_{\text{IRT}} > 1.7 \text{ \AA}$ were manually checked for systematic errors. A few additional cases with peculiar fluxes were eliminated.

The nearest LLE neighbor investigation revealed binary candidates (marked as LLE b) with more than two binary neighbors (or the first or the second neighbor is a binary), stars with continuum problems (LLE c), wavelength calibration errors (LLE w), hot stars (LLE o), stars with TiO bands (LLE t), and other types of peculiarity (LLE p).

LLE e denotes stars with no emission-type neighbors (a few hundred stars). These stars were originally included in the catalog because they are candidate members of young clusters and were tested for possibly overlooked emission, especially for cases with a faulty radial velocity shift of several 100 km s^{-1} due to very strong emission. They were removed from the sample because they do not meet the LLE selection criteria.

A cross-check using the online Simbad database for stars with available morphology types (25,238 objects) confirmed the presence of binaries, Miras (marked as “LLE t, LLE p, $J - K > 0.6$ ” in the table), Cepheids, galaxies (34 cases; most objects are actually stars with galaxies located nearby within 1 arcsec), stars of BY Dra, RS CVn and RR Lyr type, nine (micro)lensing events, red giant branch and carbon stars, gamma-ray sources, and two stars of an unknown nature. The frequency of peculiar Simbad morphology types is less than 3%. Note that spectra of RS CVn-type stars can look identical to active single stars and BY Dra stars can mimic chromospheric activity. Because the frequency of such known stars in the active sample is relatively small (13 RS CVn and 28 BY Dra objects), it is assumed that only a few individual cases could be left unrecognized in the database.

Simbad spectral types (“SimbadSpType”) available for 4691 stars uncovered B-, A-, and F-types and giants (luminosity classes I, II, and III). The rest of the spectra has a clear peak on the main sequence: most of the stars are G- and K-type dwarfs.

In total, 9138 stars were removed from the initial catalog. A list of the number of stars meeting either of the rejection criteria described above is given in Table 1.

Forty-six new active (young) candidates were found during the Simbad classification study (“T Tau,” “Pre-main-sequence,” and “Young” types). These stars were not recognized as active by the LLE technique because they do not show signs of activity or have large radial velocity shifts

Table 1
Number of Stars Eliminated from the Initial Active Candidate Catalog for Each Type of Peculiarity

Type of Peculiarity	<i>N</i>
$\log g < 3.7$	5465
LLE b	1490
Double or Binary	541 + 37
LLE e, $\log g < 3.7$	323
LLE e	194
SimbadSpType	110
LLE c	107
LLE b, $\log g < 3.7$	104
$\log g < 3.7$, SimbadSpType	59
LLE e, LLE o	56
LLE b, Binary or Double	51 + 34
LLE e, LLE b	46
$\log g < 3.7$, Double	44
Galaxy	34
LLE e, LLE o, Hot	28
$\log g < 3.7$, LLE t, LLE p, $J - K > 0.6$	27
LLE e, SimbadSpType	26
LLE c, $\log g < 3.7$	22
LLE e, $\log g < 3.7$, SimbadSpType	21
Mira	18
LLE e, $\log g < 3.7$, LLE o	14
LLE b, SimbadSpType	12
LLE e, LLE o, SimbadSpType	12
LLE t, LLE p, $J - K > 0.6$	11
BY Dra	10
Other	242
Total	9138

(not derived correctly due to their strong emission) that make them look very peculiar. However, when allowing for these radial velocity shifts, out of 46 stars, 24 were found to have $EW_{\text{IRT}} > 0.1 \text{ \AA}$ and 16 with $EW_{\text{IRT}} > 1 \text{ \AA}$.

Inspection of the new spectra, first listed in DR5, revealed new active candidates. After the removal of unsuitable cases following the same requirements as above, 2919 new spectra of 2882 stars were found to show signs of activity. The sample was added to the catalog.

An averaged spectrum in the decontaminated catalog together with 1σ and 2σ flux variations is compared with the averaged spectrum from the inactive database in Figure 4. The main contribution to the variations is a range of different atmospheric temperatures (see Section 3 for further discussion) and noise. The average 1σ variation of the continuum parts is ~ 0.02 in the middle and ~ 0.03 at the very ends of the spectrum. The value is consistent with the signal-to-noise estimation. Notable variation occurs within the strong lines, e.g., Ti I 8434.98 \AA , Fe I 8688.63 \AA , etc., due to the temperature variations of the spectra (and to a smaller extent due to metallicity).

Because marginally active stars outnumber the stars with higher emission levels due to the selection criteria, the average calcium lines almost match the inactive profiles. However, averaged spectra within the selected activity ranges (an EW_{IRT} range from 0 to 3.6 \AA with stepsize of 0.2 \AA) reveal a continuous and solid increase of excess emission fluxes (Figure 4, bottom panels), which establishes confidence in the reliability of the data. The most active averaged spectra suffer from more noise because only very few stars fall within

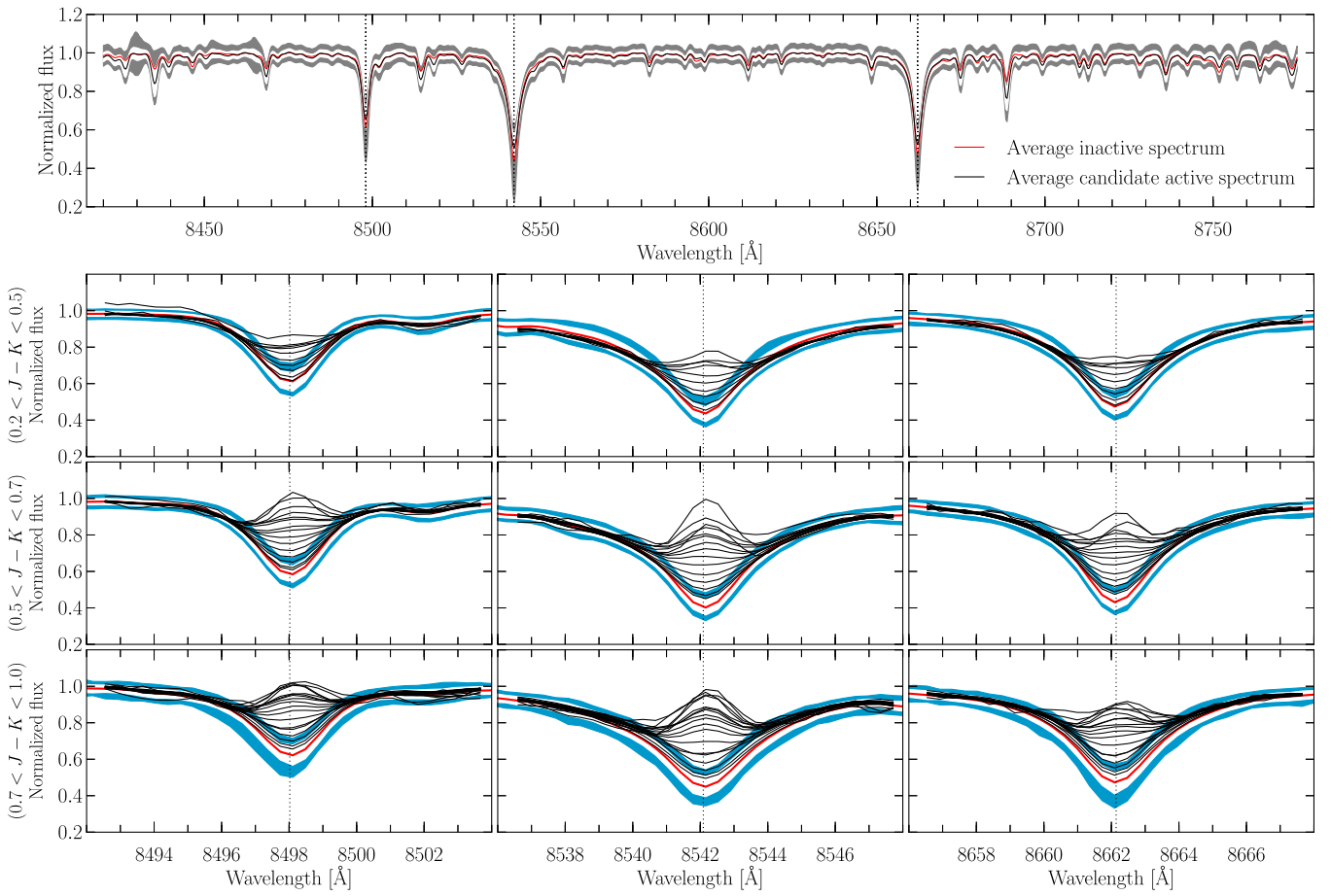


Figure 4. Top: averaged active spectrum ($EW_{\text{IRT}} > 0.1 \text{ \AA}$; black line) together with its 1σ (white) and 2σ (gray) standard deviation. Averaged inactive spectrum is shown for comparison (red line). Except for the TiO band at $\sim 8450 \text{ \AA}$ and the strongest lines (calcium excess flux, Ti I (8434.98 \AA), Fe I (8688.63 \AA), etc.), the spectra remain unchanged because the number of marginally active spectra in the active sample is large. Bottom three rows: focus on calcium lines for averaged spectra for each of the increasing activity bins (a range from 0 to 3.6 \AA with a stepsize of 0.2 \AA) divided into three color classes. For bins below 0.8 \AA , 1000 spectra are averaged. The number drops for more active spectra from few hundreds ($< 2.2 \text{ \AA}$), to few tens ($< 2.8 \text{ \AA}$), to less than 10 for the most active bins. White and blue bands indicate 1σ and 2σ standard deviations for inactive spectra and include parameter variations (metallicity and temperature to some extent within a selected color bin). Because each active spectrum was compared to its nearest neighbor (and not to an averaged inactive spectrum) the fact that the least active spectra lie within 1σ or 2σ bands does not necessarily mean that they do not differ from their inactive counterpart. For the most active spectra, line asymmetries (toward red) appear.

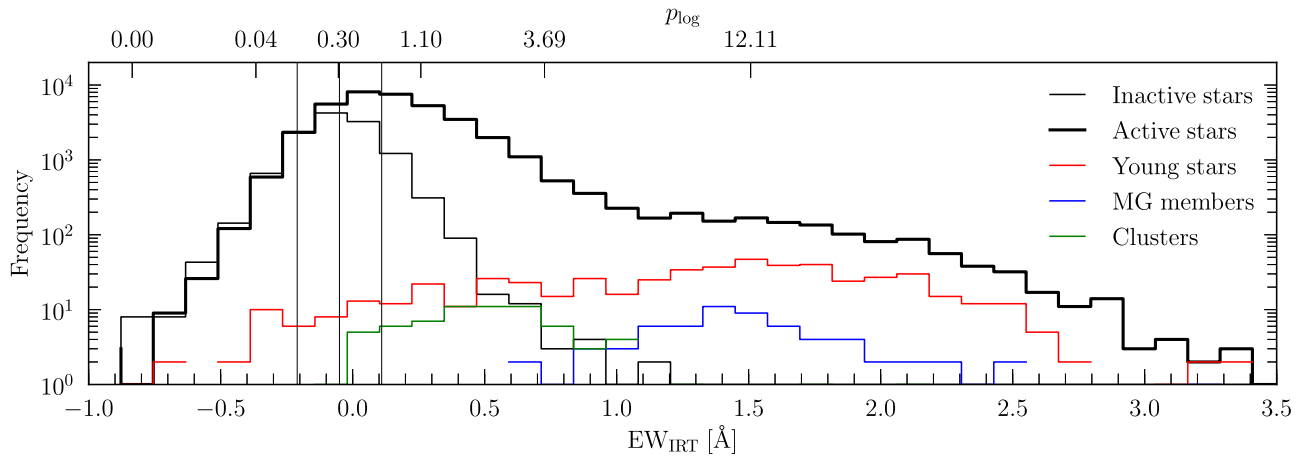


Figure 5. Distribution of activity for active candidates is bimodal (thick black line). The lower end of the less active peak overlaps with the distribution of inactive stars (thin black line) but shows a significant asymmetry with an excess of more active stars. The position of the second peak matches the distribution of young stars (red line) with Simbad morphology types “Pre-main-sequence,” “X-ray source,” “Young Object,” or “T Tau” star and the position of moving groups (MG; blue line). Cluster members are shown with the green line. Membership of MGs and clusters are listed in Table 6. The bin size is 0.12 \AA . The vertical lines show center and $\pm 1\sigma$ deviation of the distribution of inactive stars. The upper abscissa shows the probability that a star with a given activity rate and its uncertainty is more active than an inactive star (for details see Z13).

Table 2

A Comparison Between the Number of Active Candidate Stars above Selected σ Values and the Expected Number for the Unimodal Gaussian Distribution

Above σ	p_{\log}	N	Fraction	Fraction _{exp.}	$N/N_{\text{exp.}}$
$<1\sigma$	0.62	16753	0.433	0.841	0.515
$>1\sigma$	0.62	21925	0.567	0.159	3.7
$>2\sigma$	1.10	12768	0.330	0.0228	14.5
$>3\sigma$	1.77	7000	0.180	0.001	134
$>4\sigma$	2.63	3881	0.100	$3.17 \cdot 10^{-5}$	3168
$>5\sigma$	3.69	2456	0.063	$2.867 \cdot 10^{-7}$	221, 519

Note. A comparison between the number N of active candidate stars above selected σ values (probability p_{\log} is given as well) and the expected number $N_{\text{exp.}}$ for the unimodal Gaussian distribution with the average of -0.05 \AA and $\sigma = 0.16 \text{ \AA}$ (these are parameters for the inactive database activity distribution). The ratio $N/N_{\text{exp.}}$ shows that the number of active stars largely exceeds the expected number from the unimodal distribution. This is quantitative evidence for the bimodality of the distribution of active stars.

these ranges (six stars between $\text{EW}_{\text{IRT}} = 3 \text{ \AA}$ and 3.2 \AA , five stars between $\text{EW}_{\text{IRT}} = 3.2 \text{ \AA}$ and 3.4 \AA , and two stars between $\text{EW}_{\text{IRT}} = 3.4 \text{ \AA}$ and 3.6 \AA .)

Besides calcium lines, a mismatch between the averaged inactive and active spectrum occurs in other strong lines because the active database consists of cooler stars than the inactive data set (see Section 3 for the comparison).

Our new improved catalog of active candidates includes 38,678 spectra of 35,750 stars. Within the sample, the emission levels of 21,925 stars exceed $\text{EW}_{\text{IRT}} = 0.1 \text{ \AA}$ (1σ) and the activity of almost 13,000 stars surpasses the 2σ emission detection level. The distribution of activity is clearly bimodal (Figure 5). A question arises whether the more active peak at $\sim 1.5 \text{ \AA}$ is an evident feature or simply a tail of the inactive distribution enhanced by the logarithmic scale on the plot. A comparison of the expected fraction of stars (a single Gaussian distribution centered at -0.05 \AA and with $\sigma = 0.16 \text{ \AA}$ that corresponds to the inactive sample) and the actual fraction of stars (Table 2) strongly supports the hypothesis of the bimodal distribution. The less active peak is composed of stars with undetectable emission and a moderately active group of stars above $\text{EW}_{\text{IRT}} = 0.1 \text{ \AA}$. Its skewness does not originate in the imposed tail of the more active peak but stands on its own: the amplitude of the more active peak is ~ 100 but at $\text{EW}_{\text{IRT}} = 0.4 \text{ \AA}$ there are a few thousand more stars than expected. The existence of bimodality is already known in the literature for the Ca II H&K lines (e.g., Henry et al. 1996).

The more active peak overlaps with the distribution of RAVE stars marked as young, T Tauri or pre-main-sequence types in the Simbad database. Since the active catalog contains a relatively large number of such young stars (~ 1600 stars with $\text{EW}_{\text{IRT}} > 1 \text{ \AA}$, which is 4% of the active sample), the further analysis in this paper is focused on the most active spectra.

3. COLORS OF ACTIVE STARS

Besides the 2MASS J and K_s magnitudes (Skrutskie et al. 2006; 94% of J magnitude uncertainties and 96% of K magnitude uncertainties below 0.03 mag for active RAVE stars), additional data were acquired to better characterize the nature of emission objects. The catalog is supplemented by N_{UV} fluxes from the GALEX Survey (Bianchi et al. 2011; 1771–2831 \AA ; 50% of stars with uncertainties below 0.04 mag and 80% below 0.1 mag), ROSAT X-ray flux data

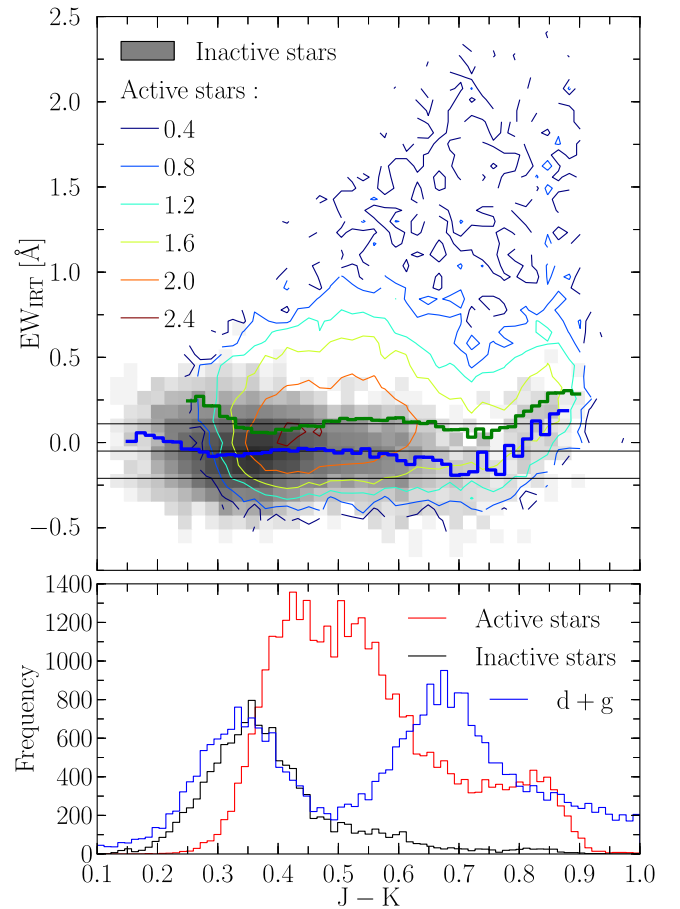


Figure 6. Top: activity vs. $J - K$ color for active (contours; the number of stars per bin) and inactive stars (gray shades). Both scales are logarithmic. The highest activity rates are most likely to occur in stars redder than the Sun ($(J - K)_{\odot} = 0.36$). Stars above $J - K > 0.7$ show a correlation of activity rate with color (the thick blue line represents the average activity of active stars and the thick green line the average activity of inactive stars). Horizontal black lines indicate the center and $\pm 1\sigma$ deviation of the EW_{IRT} distribution of inactive stars. Bottom: distribution of $J - K$ for active (red line) and inactive stars (black line). Most of the inactive stars ($\sim 12,000$ objects in total) are solar-like while the majority of active stars are cooler (94% below 5700 K and 45% below 5000 K). A slight jump occurs just above $J - K = 0.5$ in the active distribution: because at low Galactic latitudes only stars with $J - K > 0.5$ were observed, the number of red stars is increased. A large number of the coolest (M-type) stars accumulate at $J - K \approx 0.8$. The blue line represents 35,000 randomly chosen RAVE stars (including giants—mostly red clump; histogram values are only qualitative and not to scale with the y-axis).

(0.1–2.4 keV; Voges et al. 1999), WISE W_1 and W_2 mid-infrared bandpasses (3.4 and 4.6 μm ; Cutri et al. 2014; typical W_1 uncertainties are 0.023 and typical W_2 uncertainties are 0.020), and Landolt V magnitudes from the APASS database (typical uncertainties 0.02 mag; Henden & Munari 2014).

A cross-match between RAVE and the GALEX and WISE catalogs was performed by the X-match online application (criterion of 5 arcsec radius). A manual coordinate match was used for the APASS catalog with 3 arcsec as a maximum distance between APASS and RAVE stars (the typical APASS astrometric uncertainty is 0.17 arcsec, the fiber size in RAVE is 6.7 arcsec). X-ray sources were identified via ROSAT 1RXS names obtained through the Simbad online database. It is likely that many of the sources were overlooked but a direct coordinate match was not reliable due to large positional errors in the ROSAT data (10 arcsec).

The $J - K$ colors of the majority of active stars lie between the solar value (0.36) and ~ 0.7 (Figure 6, lower panel) while the inactive database is solar-like. A bump at $J - K \sim 0.55$ in the color distribution of the active sample originates in the fact that a color cut was performed in the Galactic plane ($|b| < 25^\circ$) at $J - K = 0.5$ in order to observe more red giants when the RAVE observations were defined. The distribution at $J - K > 0.5$ is thus more populated.

A number of red stars is concentrated around $J - K \sim 0.8$. The reader may recall the additional observations of the Aquarius stars described in Section 2.1. However, since there are 715 Aquarius red active stars observed out of 6774 red ones in total (11%), this is not the main contribution to the population.

The nature of red stars is revealed by the the mid-infrared WISE photometry (Figure 7, panel (d)). Objects with $J - K > 0.7$ and $-0.1 \lesssim W_1 - W_2 \lesssim 0.2$ are cool (probably M-type) dwarfs. A similar analysis separating cool giants and dwarfs was done by Li et al. (2016). A comparison between the active (black contours) and inactive sample (gray contours) shows a relative lack of cool inactive dwarfs because the majority of stars is active in this region of the color-color diagram. A number of very active stars at $J - K \approx 0.7$ is concentrated around $W_1 - W_2 \approx 0$. Dashed contours representing giants (30,000 randomly chosen RAVE stars with $\log g < 3.5$ and $T_{\text{eff}} < 6000$ K) do not overlap with the very active area. This fact, together with the distribution of giants over $J - K$ compared to the distribution of the active sample (Figure 6), excludes the possibility that the very active stars are mistaken for the old red clump giants.

A similar diagram (left column—panels (a)–(c)) is shown using the near-ultraviolet photometry ($N_{\text{UV}} - V$ colors). In both cases (near-ultraviolet and mid-infrared colors), stars with modest and moderate activity ($\text{EW}_{\text{IRT}} < 0.5 \text{ \AA}$) appear to have colors similar to inactive stars. However, the most active stars with $J - K > 0.6$ are significantly blueshifted in $N_{\text{UV}} - V$ and redshifted in $W_1 - W_2$. The bigger the offset from the main sequence, the more active the star is on average.

A comparison between colors of active spectra and their first nearest inactive neighbors shows that stars above $\text{EW}_{\text{IRT}} > 1 \text{ \AA}$ display a slight offset toward the red in the $J - K$ color (0.07 ± 0.10) and a remarkable ultraviolet (-0.93 ± 1.019 offset toward the blue in the $N_{\text{UV}} - V$ color) and infrared excess (0.037 ± 0.079 offset in the $W_1 - W_2$ color). It is not entirely clear whether the red offset originates in the near-infrared excess emission or reddening. A great fraction of active stars reside in the Galactic plane and some of them might still be embedded in their birth cocoons, but in general distances to dwarfs are less than 400 pc due to the observational luminosity limit in RAVE. Zuckerman & Song (2004, p. 686) state that for classical T Tauri stars (pre-main-sequence stars less than a few million years old and associated with interstellar nebulosity), “[e]xcess emission above photospheric emission at near-, mid-, and far-infrared wavelengths suggests the presence of substantial quantities of nearby heated dust particles in the form of a disk or envelope or both. Ultraviolet line and continuum emission of classical T Tauri stars indicates that, typically, they are actively accreting a portion of the surrounding gas and dust.” On the other hand, Zuckerman & Song (2004, p. 686) say, “by an age of ~ 10 Myr, stellar optical activity is much reduced and near- and mid-infrared excesses are very infrequent.” Dusty circumstellar

disks (around pre-main-sequence stars) and their infrared emission are discussed in detail by Zuckerman (2001).

According to Feigelson & Montmerle (1999), the X-ray emission is an ubiquitous characteristic of young low-mass stellar objects from protostars with $\sim 10^5$ years to stars approaching the zero-age main sequence (ages of 10^7 years) as a consequence of powerful magnetic reconnection flares. It is thus no surprise that very active red stars exhibiting X-ray flux overlap with the most active region of the diagrams. What is more, RAVE stars with $\text{EW}_{\text{IRT}} > 1 \text{ \AA}$ identified in the Simbad database as pre-main-sequence, T Tauri, and young objects, together with objects younger than 100 Myr (identification is given in the Appendix, Table 6), reside in the same active part of the plots. Members of clusters, moving groups, and associations are plotted for comparison.

The consistency of the photometric data justifies the assumption that the majority of the stars off the main sequence in the $N_{\text{UV}} - V - J - K$ and $W_1 - W_2 - J - K$ planes (i.e., very active stars with $\text{EW}_{\text{IRT}} > 1 \text{ \AA}$) are very young, possibly still residing on the Hayashi tracks. The sample traces stars originating from recent star formation events in the solar neighborhood. The reader may recall that active RAVE objects are field stars with a random selection function. Since the active catalog consists of a great fraction of Tycho-2 stars in the solar neighborhood, it is expected that parallaxes provided by *Gaia* will enable their precise placement on the isochrones. Besides the study of activity on the pre-main sequence, the position on the isochrones will help to investigate the nature of solar-like active objects with $(J - K) < 0.5$. They reach activities of up to $\sim 1 \text{ \AA}$ and do not photometrically differ from inactive stars (except for a mild redshift in $J - K$) despite their young age. They evolve faster since their mass is greater than the mass of late-type stars. Moreover, the nature of the generation of a magnetic dynamo might depend on stellar mass and the relative depth of the convective envelope.

Activity of cool dwarfs ($J - K \geq 0.7$) increases on average with redder color (upper panel of Figure 6: green line for active stars and blue for the inactive sample). Apart from the color-color diagrams, cumulative distributions over EW_{IRT} for subsets within selected color ranges (Figure 8) confirm that the more active peak in the distribution consists mainly of red stars. The redder the population, the more active the stars. Only the bluest stars have their distribution centered below $\text{EW}_{\text{IRT}} = 0.1 \text{ \AA}$ (1σ above the center of the reference inactive distribution). The distribution spreads out toward higher activities above $J - K > 0.7$. A significant fraction (20%) of stars with $0.85 < J - K < 0.9$ is more active than 1 \AA as predicted earlier from the red sample.

According to the literature (e.g., R84) there exists a lower color-dependent boundary of the total surface flux in the Ca II H&K lines of the main-sequence stars that corresponds to the basal emission of the star. The basal activity remains constant for solar-like stars while emission values between $1 < B - V < 1.6$ are increased (Isaacson & Fischer 2010). The region with higher basal levels corresponds to $0.65 < J - K < 1$, which could explain the $\text{EW}_{\text{IRT}} - J - K$ relation.

However, basal emission is also expected to be present in the inactive sample as it is found in all stars with convective envelopes. This component should thus already have been eliminated from the EW_{IRT} by the spectral subtraction technique assuming that active and inactive spectra represent

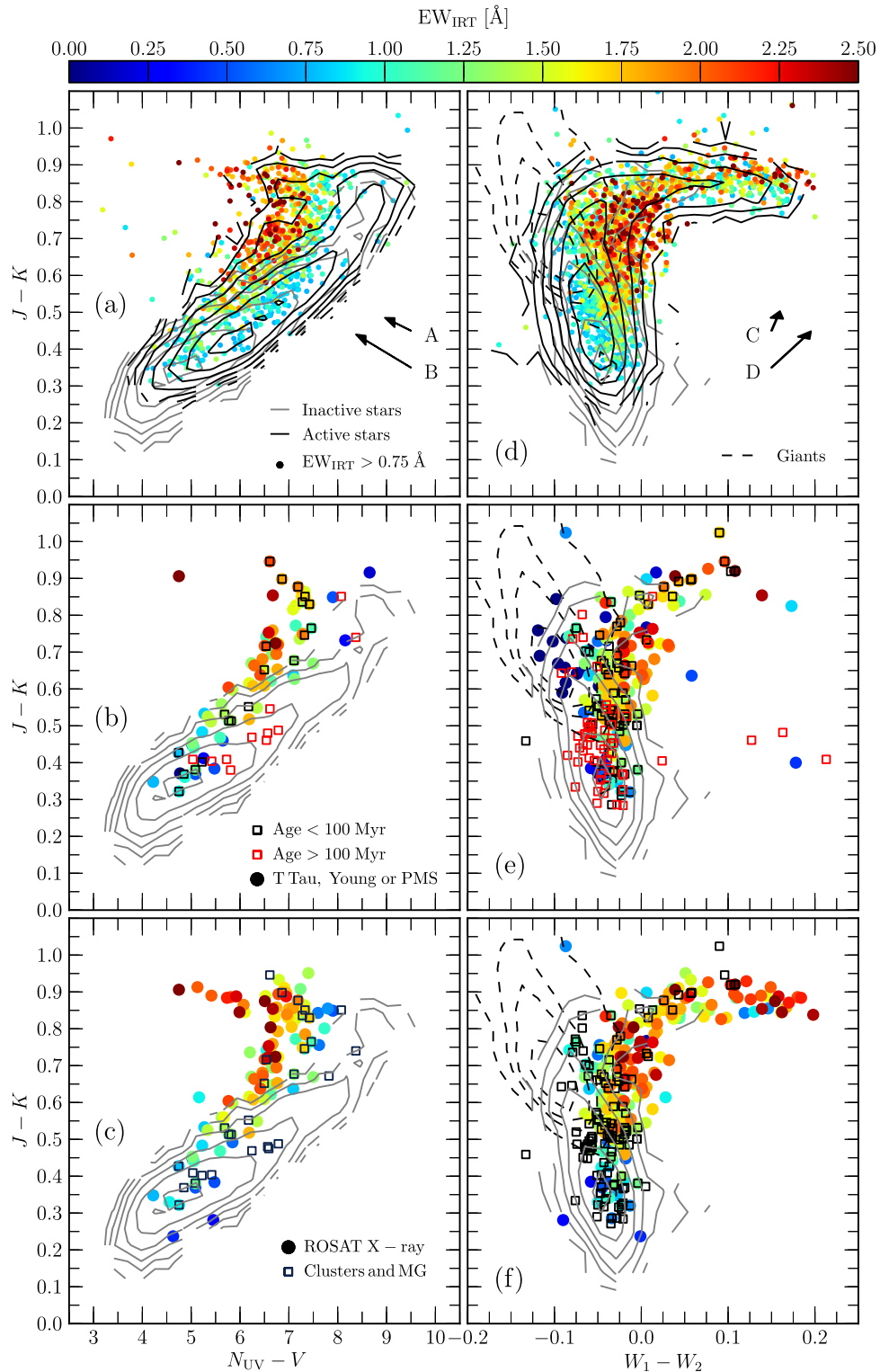


Figure 7. $J - K$ vs. $N_{UV} - V$ (left) and $W_1 - W_2$ (right) diagrams for active stars. Gray contours represent the reference distribution of inactive stars (i.e., the main sequence) in all panels. All contours are plotted in a logarithmic scale. Panels (a) and (d): the distribution of all active candidates (black contours); stars with $EW_{IRT} > 0.75$ Å are additionally illustrated with dots. Note a concentration of the most active stars at $J - K > 0.7$ and $5 < N_{UV} - V < 8$ ($W_1 - W_2 \approx 0$) and the fact that the most active stars in panels (a)–(c) lie off the main sequence. Arrows indicate the average shift in comparison with the colors of the first inactive nearest neighbors of stars for activities between 0.5 and 1 Å (A and C) and above 1 Å (B and D). The legend in the left panel represents symbols used in both near-ultraviolet and mid-infrared plots. The distribution of giants (dashed contours; only the densest regions are shown) is given for reference. Panels (b) and (e) show young stars (dots; according to Simbad) and stars with known ages (see Table 6), while X-ray sources, and cluster and moving group members are depicted in panels (c) and (f). Simbad stars showing reliable indicators of youth overlap with the most active RAVE stars and demonstrate their young ages. For more details, see the text.

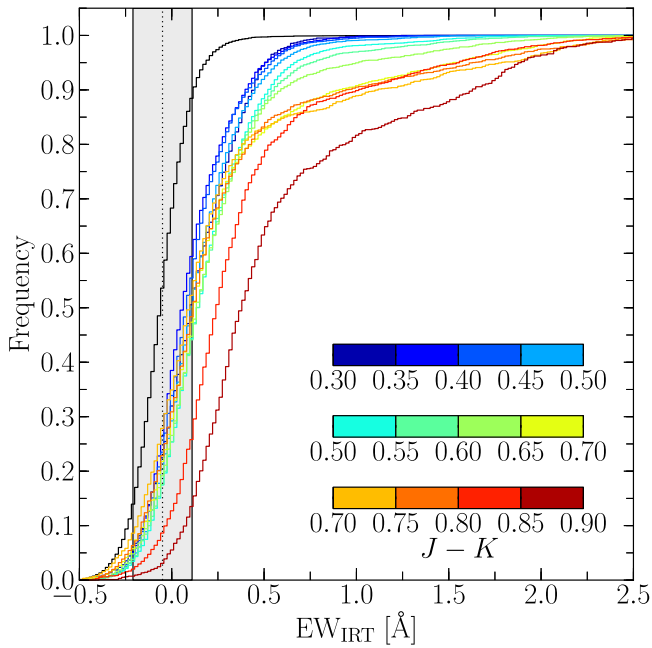


Figure 8. Cumulative distribution of activity for selected $J - K$ color ranges. The redder the population, the higher the probability for activity and, at the same time, higher activity rates. The gray vertical band indicates the center and $\pm 1\sigma$ deviation of the activity distribution of inactive stars (depicted by the black curve).

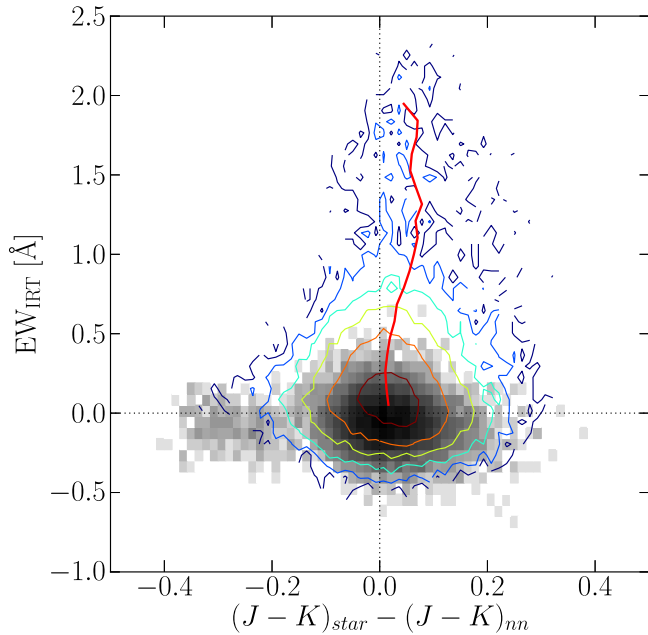


Figure 9. EW_{IRT} vs. $J - K$ color excess for active stars (contours). The latter is given as a difference between the color of the star and the color of its nearest inactive neighbor, assuming that reddening of inactive stars (gray histogram) is negligible. The red vertical solid line marks the average color excess at the given activity rate (the bin size is 0.11 \AA). The majority of stars are concentrated around zero color excess. Very active stars are prone to mild reddening (or infrared excess emission) because they mostly reside in the Galactic plane and are possibly still embedded in their gas and dust cocoons (pre-main-sequence stars).

similar stars. Nonetheless, EW_{IRT} increases with color not only for active stars but for the inactive sample as well, despite the fact that a star and its nearest inactive neighbor have almost identical colors (i.e., should have similar spectra) as shown in

Figure 9 (note that the nearest neighbor search was based solely on the normalized spectrum; other parameters (e.g., colors) were excluded). The activity of inactive red stars is on average lower than the emission levels of red active stars. The reason for the marginal activity detected in the red spectra of the inactive sample is due to relaxed selection criteria in the coolest part of the set. As shown in Figure 8 the redder the star, the more likely it appears to be active. At the same time, if nearest inactive neighbors in the EW_{IRT} determination of active stars exhibit mild excess emission, the EW_{IRT} of red active stars is underestimated. Mild activity of the inactive database is certainly one of the disadvantages of the spectral subtraction technique. Nevertheless, it seems that the trend of increasing activity with color cannot be explained by the basal emission. Other underlying phenomena, perhaps connected to the nature of convection and the generation of magnetic fields in the coolest (and youngest) stars, must be present.

4. AGE-ACTIVITY RELATION

The age of a star cannot be measured directly. It can only be estimated using various indirect (possibly distance-independent) methods. For pre-main-sequence stars the lithium 6708 \AA depletion boundary is used (e.g., Jeffries 2014) while gyrochronology exploits the inverse correlation between the age and the rotation rate for main-sequence F, G, K, and early M stars (Barnes 2007). Astroseismology proved very successful for pulsating stars but it is not entirely clear if the detection of pulsations in stars cooler than the Sun is possible (Huber et al. 2011). Due to the absence of sensitive indicators, the evaluation of the main-sequence field star ages remains fundamentally difficult.

Young solar-type stars appear to be more magnetically active than older, evolved stars. The magnetic activity level correlates with a diminishing stellar rotation rate through coupling by the magnetic dynamo effect (Skumanich 1972; Noyes et al. 1984, Baliunas et al. 1995). Skumanich (1972) studied cluster members and binary companions of more massive stars and reported the relationship between stellar age and chromospheric emission decay to be proportional to $\tau^{-1/2}$. Many authors later calibrated the power-law relationship with their samples and ages provided by other, alternative methods. While Stelzer et al. (2013) confirm the relation for G, K, and M dwarfs, M08 review calibrations from the literature (Barry et al. 1987; Soderblom et al. 1991; Lachaume et al. 1999) and describe their new empirical calibration for the Ca II H&K, reliable for solar-type (F7-K2) stars between 0.6 and 4.5 Gyr:

$$\log \tau = -38.053 - 17.912 \log R'_{\text{HK}} - 1.6675 (\log R'_{\text{HK}})^2. \quad (1)$$

Here R'_{HK} is a ratio between the sum of emission fluxes in the Ca II H&K lines (bandwidth of 1 \AA) and the bolometric flux of the star.

The nature of the chromospheric activity evolution has been examined by various authors, e.g., Pace (2013), Zhao et al. (2011), and Lyra & Porto de Mello (2005). A comparison of the age-activity relation as a dating technique with other methods for young stars (lithium depletion boundary and gyrochronology) was described by Jeffries (2014). Soderblom (2010) comprehensively reviews stellar dating techniques and provides advantages and disadvantages of using the activity-age relation. He emphasizes the fact that the main parameter is stellar rotation. Its relation to activity is poorly understood as it

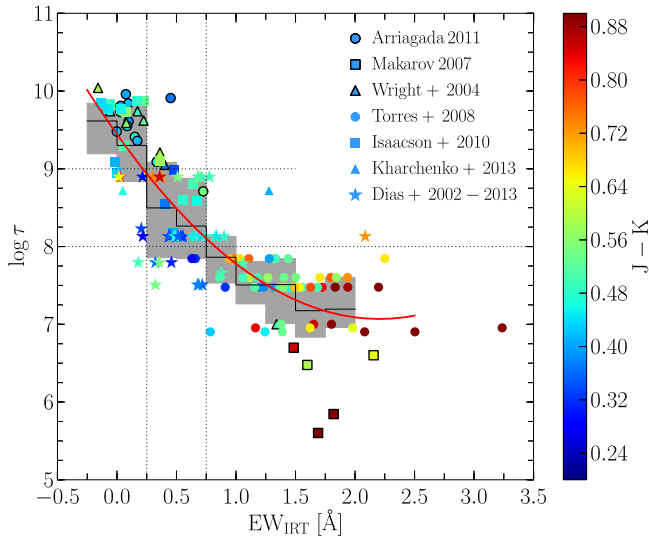


Figure 10. Calibration of the age– EW_{IRT} relation (red line). Ages (logarithmic scale, $\log \tau$) from external catalogs are shown against their EW_{IRT} values (dots). The colors indicate $J - K$ indices; the scale is given in the color bar on the right. A moving average of $\log \tau$ shows a steady decline of activity with age (black line; gray area is 1σ standard deviation). Dotted lines mark three main age–activity regimes: ≥ 1 Gyr ($EW_{\text{IRT}} < 0.25 \text{ \AA}$), between 0.1 and 1 Gyr ($0.25 \text{ \AA} < EW_{\text{IRT}} < 0.75 \text{ \AA}$), and younger than 100 Myr ($EW_{\text{IRT}} \geq 0.75 \text{ \AA}$).

turns out that—especially for the pre-main-sequence and zero-age main-sequence stars—a given rotation rate can result in a range of activity levels. Gallet & Bouvier (2013) show the relation converges only after ~ 500 Myr. An approximate tuning is possible for stars between 500 Myr and 1.5–2 Gyr. Stars later remain active but it is more difficult to detect their diminishing low levels of activity. A large spread in rotational velocities of the youngest stars disproportional to their ages escalates the complexity of the problem besides the evidence that high rotation rates with longer convective turnover times at lower masses and pre-main-sequence stars cause saturation of chromospheric activity indicators. The activity lifetime of stars of the latest types (M3–M5) is increased, possibly because of an onset of the full convection and different dynamo mechanisms (West et al. 2008). For solar-type stars older than ~ 500 Myr accurately measured $\log R'_{\text{HK}}$ values yield $\log \tau$ to ± 0.2 dex—the precision is $\pm 60\%$ (M08). The uncertainty grows for younger stars and dating becomes useless below 100 Myr where only upper age limits can be provided.

The influence of metallicity on the absorption line depths makes activity indices based on the ratio of Ca II H&K flux and continuum (e.g., the S index, Vaughan et al. 1978 and $\log R'_{\text{HK}}$, Noyes et al. 1984) metallicity dependent (Rocha-Pinto & Maciel 1998). This effect is reduced in the RAVE active catalog with the spectral subtraction technique. However, lower abundances might affect the dynamo itself and the generation of the heating.

4.1. Age– EW_{IRT} Calibration

Ages of RAVE stars have been estimated by Binney et al. 2014. Because their age prior was focused mainly on older stars, active stars are estimated to be older than a few Gyr. In our work, reference ages of known Galactic open cluster members, moving groups, and ages derived from the Age– $\log R'_{\text{HK}}$ relation are used (see Table 6 for references and additional info).

Table 3

Average Age within the Activity Interval of the Reference Stars with Known Age (Figure 10)

$EW_{\text{IRT},1} (\text{\AA})$	$EW_{\text{IRT},2} (\text{\AA})$	$\log \tau$
–0.25	0.0	$9.62^{+0.23}_{-0.42}$
0.0	0.25	$9.30^{+0.52}_{-0.47}$
0.25	0.5	$8.50^{+0.59}_{-0.64}$
0.5	0.75	$8.26^{+0.62}_{-0.42}$
0.75	1.0	$7.86^{+0.27}_{-0.31}$
1.0	1.25	$7.51^{+0.30}_{-0.24}$
1.25	1.5	$7.51^{+0.34}_{-0.50}$
1.5	1.75	$7.18^{+0.33}_{-0.34}$
1.75	2.0	$7.19^{+0.41}_{-0.24}$

Despite the many limitations described in the previous section and considerable scatter of the data, the large-scale correlation between activity and age is still evident in RAVE (Figure 10). It allows us to provide a coarse calibration. The goal of this work is not precise dating but a relation that gives an order of magnitude age estimate that can significantly contribute to the establishment of young candidate lists in large field star surveys.

A moving mean of the ages within activity bins (0.25 \AA) up to 2 \AA is presented together with the $\pm 1\sigma$ deviations in Table 3. Since this is an approximate relation we assume that more active stars are not older than a few tens of millions of years.

The ages of the oldest and the least active reference stars coming from the catalogs with known $\log R'_{\text{HK}}$ –age relation values reach a few billions of years. The Solar $\log R'_{\text{HK}}$ activity is ~ -4.9 (M08) which translates to $-0.2 \text{ \AA} < EW_{\text{IRT}} < 0.2 \text{ \AA}$ according to the $\log R'_{\text{HK}}$ – EW_{IRT} correlation in Figure 7 in Z13. The age of a star within this activity bin is between 1 and 6 Gyr.

Regarding the discussion in Section 3, spectra with activity above $\sim 1 \text{ \AA}$ and $J - K \gtrsim 0.5$ probably belong to the pre-main-sequence population of stars and they must thus be younger than ~ 100 Myr. The more active peak in the activity distribution occurs around 1.5 \AA , which translates to a few tens of millions of years. Although emission levels below $\sim 1 \text{ \AA}$ on average correspond to ages older than 100 Myr, the distribution of activity of young stars with $J - K < 0.5$ extends down to $\sim -0.5 \text{ \AA}$. The relation is color dependent, as pointed out by many authors, e.g., M08. Nevertheless, the correlation between age and activity in Figure 10 does not show any particular color trend. The reason is probably a combination of the fact that most of the calibration stars are solar-like with $J - K < 0.5$ and that the scatter is too large.

A parabola was used to find the age of a star for a given activity level, as follows:

$$\log \tau = 0.49 \text{ \AA}^{-2} EW_{\text{IRT}}^2 - 2.15 \text{ \AA}^{-1} EW_{\text{IRT}} + 9.44. \quad (2)$$

The fit is only informative. Clearly, the uncertainties of the derived ages from the equation are large and this method is not to be used for precise dating. Due to the large scatter of the data used in this paper, only a categorization of ages into three orders of magnitude is possible: ages of stars with $EW_{\text{IRT}} < 0.25 \text{ \AA}$ are estimated to be 1 billion years or greater. Stars with activity levels between 0.25 and 0.75 \AA are estimated to be between 0.1 and 1 Gyr old whereas the most

Table 4
Description of the Columns in the Data Table

Column	Units	Description
RA	deg	R.A. (J2000.0)
DE	deg	Decl. (J2000.0)
S/N	...	Signal-to-noise ratio of spectrum
EW _{IRT}	Å	EW _{IRT}
eEW _{IRT}	Å	Uncertainty of the EW _{IRT}
LogAge	...	log τ estimate from the age–activity relation

active stars ($EW_{IRT} \geq 0.75 \text{ \AA}$) are younger than 100 Myr. Nevertheless, the result is highly beneficial in large surveys for the identification of a large number of young stars that are candidates for further more detailed investigation using alternative methods.

The catalog of active stars will appear online in the VizieR database. The description of the columns including the age estimate is given in Table 4.

5. RAVE DISTANCES

The number of all active stars over the number of all RAVE dwarfs with $\log g > 3.75$ (Figure 11) indicates that star formation mainly occurs in the Galactic plane, as expected. Additionally, a plot of the ratio between the number of active stars over the number of all observed RAVE dwarfs for three color classes versus the Galactic latitude (Figure 12, panels (a)–(c)) demonstrates that the most active stars (red line) are most probably found closer to (and in) the Galactic plane. However, because the stars at low latitudes can theoretically still lie at great distances from the Galactic plane z , it is more convenient to plot the distribution over z .

Spectrophotometric distances to the RAVE stars have been estimated using an updated version of the Binney et al. (2014) distance pipeline, which includes a wider range of metallicities (the lower limit was extended from $[Fe/H] = -0.9$ in the previous version down to -2.2 dex) in the adopted isochrones. A comparison of distances from RAVE and external catalogs (for cluster and moving groups members) shows an offset (the average difference between distances for a particular star closer than 500 pc is 31 pc) and a rather big scatter (standard deviation of the difference between the estimates is 98 pc and 36 pc for stars closer than 100 pc). A color–magnitude diagram using RAVE distances reveals that a large fraction of very active stars (above $J - K > 0.6$) reside either above giants (their surface gravity is typically underestimated) or below the main sequence.

To overcome the overall problem of distances, stars were confined between a 1 Gyr isochrone on the main sequence and a 10 Myr isochrone in the pre-main-sequence zone (it corresponds to $\sim 1.5 M_{\odot}$ main-sequence turn-on initial mass; more massive stars have already settled on the ZAMS while stars below this point are still contracting). The latter age is likely underestimated but it serves as the lower limit. Theoretically, for the reddest stars the two distances differ by a factor of ~ 1.7 , and for the bluest stars by a factor ~ 1.9 . Both isochrones use Padova models (PARSEC release v1.2S; Bressan et al. 2012); the metallicity is set to the solar value.

The detection limit for K4-type RAVE dwarfs is around 200 pc (~ 400 pc for solar-like dwarfs). The vertical scale height of the Galactic thin disk is ~ 300 pc (Freeman & Bland-Hawthorn 2002), which means that practically all active

candidates are expected to be situated within this layer. Due to the I magnitude being the only limit outside the color-selected Galactic plane, populations of RAVE stars with similar spectroscopic types should in principle occupy volumes in space of similar size. For this reason the data analysis was performed for three different color ranges. Moreover, active stars were divided into two groups: less active stars with $EW_{IRT} < 1 \text{ \AA}$ and more active stars with $EW_{IRT} \geq 1 \text{ \AA}$. Distances for inactive stars are not considered because of the selection criterion: very high signal-to-noise values of template spectra were demanded when building the inactive database, which effectively means that these stars must reside very close to the Sun.

At 1 Gyr (Figure 12, panels (d)–(f)) more active stars (especially solar-like ones with $0.2 < J - K < 0.5$; panel (d)) on average have smaller distances than less active stars. There is no reason for their absence at greater distances. As it is evident that the more active stars might still reside in their pre-main-sequence phases, the problem can be solved by raising the most active subset to younger and more luminous isochrones as stellar distance in the Hertzsprung–Russell diagram grows in the direction toward the giants. The red line in the plot represents the distance distribution for more active stars at 10 Myr. Although distances for both activity groups with $J - K > 0.5$ (panels (e) and (f)) at 1 Gyr are comparable, distances for more active stars at 10 Myr are expectedly larger. However, it seems that the distance distribution for very active solar-like stars ($0.2 < J - K < 0.5$; panel (d)) is in disagreement with their placement on the color–color diagram (Figure 7). Photometry shows that this group of stars is placed on the main sequence (so they must be put on the 1 Gyr isochrone). One might think that the possible reason for the lack of more distant stars could be the detection limit of activity: because solar-like stars show lower levels of emission, its detection is more challenging in noisy spectra, i.e., spectra of more distant stars. Nevertheless, this is not the case since the distribution of less active stars reaches greater distances.

In order to better understand the distance distribution of the youngest RAVE stars, the population synthesis code Galaxia (Sharma et al. 2011) was used to produce a mock-RAVE catalog (Wojno et al. 2016). First, a full-sky synthetic catalog was generated with an apparent magnitude limit $0 < I_{DENIS} < 14$. These apparent magnitudes were corrected for extinction using Schlegel map values (Schlegel et al. 1998) at the position of the star, and modified to include errors using a RAVE-like magnitude error distribution. The RAVE selection function ($S_{\text{select}} \sim (l, b, I_{2\text{MASS}}, J - K_s)$) was then applied to this sample to match the distribution of the observed RAVE stars. Because it is evident that active stars are rare in the blue part of RAVE’s main sequence, the upper log g limit was set to 4.4 and $T_{\text{eff}} < 6000$ K. All stars on the lower main sequence satisfying these criteria are included in the mock sample because activity is not simulated in the catalog. Further, only the youngest stars were selected from the set: stars below $\log age = 7.78$ (purple shade in the plot; this age limit corresponds to $EW_{IRT} > 1 \text{ \AA}$ according to Equation (2)) and stars with $7.78 < \log age < 9.23$ ($0.1 \text{ \AA} < EW_{IRT} < 1 \text{ \AA}$; green line). In order to additionally divide the sample into three color classes the temperature was converted to $J - K$ colors (stars with $T_{\text{eff}} > 5100$ K correspond to $J - K < 0.5$, stars with $4500 \text{ K} < T_{\text{eff}} < 5100 \text{ K}$ to $0.5 < J - K < 0.7$, and stars cooler than 4500 K to $J - K > 0.7$).

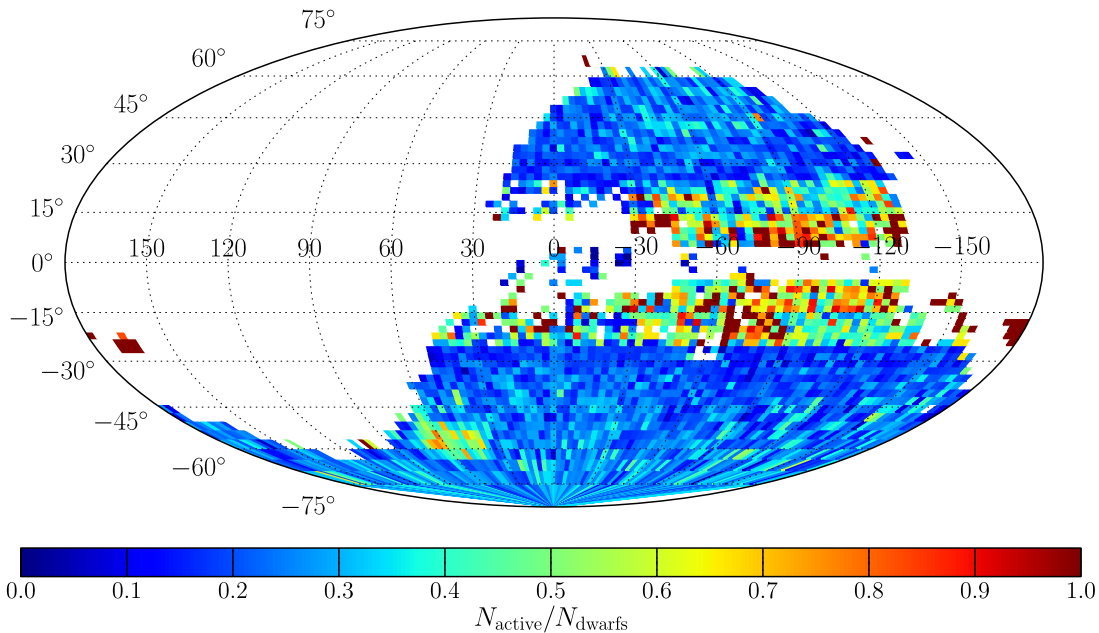


Figure 11. Number of all active candidates over the number of all RAVE dwarfs with $\log g > 3.75$. The occurrence of activity is high in the Galactic plane, partly because of the color cut $J - K > 0.5$ performed at $25^\circ < |b|$. An overdensity of active stars in the direction of the Aquarius constellation ($35^\circ < l < 75^\circ$ and $-62^\circ < b < -50^\circ$) is seen due to additional color-limited observations of the Aquarius stream.

A qualitative comparison between the observed and mock catalog distributions shows similar trends. The lack of more distant, very young stars in the bluest sample ($0.2 < J - K < 0.5$; panel (d)) is also evident in the mock sample. The nonexistence of distant, very young stars in the mock catalog as well excludes the selection effect in the observed RAVE sample.

Note that there is a quantitative difference present between the mock and observed data set. A possible reason is that Galaxia does not inherently include errors on distances, and that isochronal estimates in this work do not take extinction into account.

Despite the efforts to estimate stellar distances, their values remain unreliable and inconclusive. For this reason we skip the study of the distribution of stars over the distance from the Galactic plane z . Accurate and precise parallaxes from the *Gaia* catalogs will provide more detailed insight into the distribution of active stars over the distance from the Galactic plane.²¹

6. DISCUSSION AND CONCLUSIONS

This work reports on the improved identification of stellar activity in the catalog introduced by Z13 and extends its quality control. Over 9000 unreliable or improper spectra were removed from the sample (Section 2). Two thousand nine hundred nineteen new spectra of 2882 stars published for the first time in DR5 were found to show signs of activity and were added to the active catalog. The increasing excess emission flux in the Ca II IRT in the averaged spectra for each activity bin from levels below the detection limit to individual cases with emission filling in calcium lines confirms the reliability of the data (Figure 4). The new catalog comprises of 38,678 candidate spectra with activities of almost 13,000 stars above 2σ and almost 22,000 stars above the 1σ emission detection level.

²¹ Note to the reader: this paper was submitted before the TGAS catalog (*Gaia*-DR1) was released.

The distribution of activity is bimodal (Figure 5). This statement is supported by the comparison of the active sample and a single Gaussian function equivalent to the distribution of inactive stars. Since the number of stars around the peak at $\sim 1.5 \text{ \AA}$ exceeds the expected number by a few thousand times (Table 2), this is clear evidence for the existence of an additional peak in the distribution. Bimodality was also known to appear in the distribution of emission in the Ca II H&K lines but the reason for the two peaks is not entirely clear. Since Gray et al. (2006) report a disappearing bimodality for stars with $[M/H] < -0.2$, different dynamo-generating mechanisms combined with metallicity dependence and stellar evolution might play a role in the structure of stellar magnetic fields and the resulting excess emission flux. A promising upcoming detailed chemical abundance information of up to 30 elements for ~ 1 million stars from the Galah Survey with a precision of < 0.1 dex (De Silva et al. 2015) and with a combination of H α and H β emission looks suitable to help disentangle the underlying processes.

An interesting phenomenon in the distribution of active stars in the EW_{IRT} versus $J - K$ space is observed (Section 3). Above $J - K > 0.7$, the average activity is not only the highest but correlated with color as well (Figure 6). The contribution of the color-dependent basal emission is excluded from the EW_{IRT} by the spectral subtraction technique using a measured inactive template database. A similar trend is observed in the sample of inactive stars (a small fraction of the coolest marginally active stars was recognized as inactive because of relaxed selection criteria due to the lack of inactive red stars). Further photometric investigation (Figure 7) unveiled their position off the main sequence in both the $J - K - N_{UV} - V$ and $J - K - W_1 - W_2$ space, exposing a large near-ultraviolet and mid-infrared excess emission. Pre-main-sequence, T Tauri, and young stars together with X-ray sources (additional data from the Simbad database) and stars younger than 100 Myr (see the Appendix for the age reference) overlap with these regions. Undoubtedly, red and very active stars

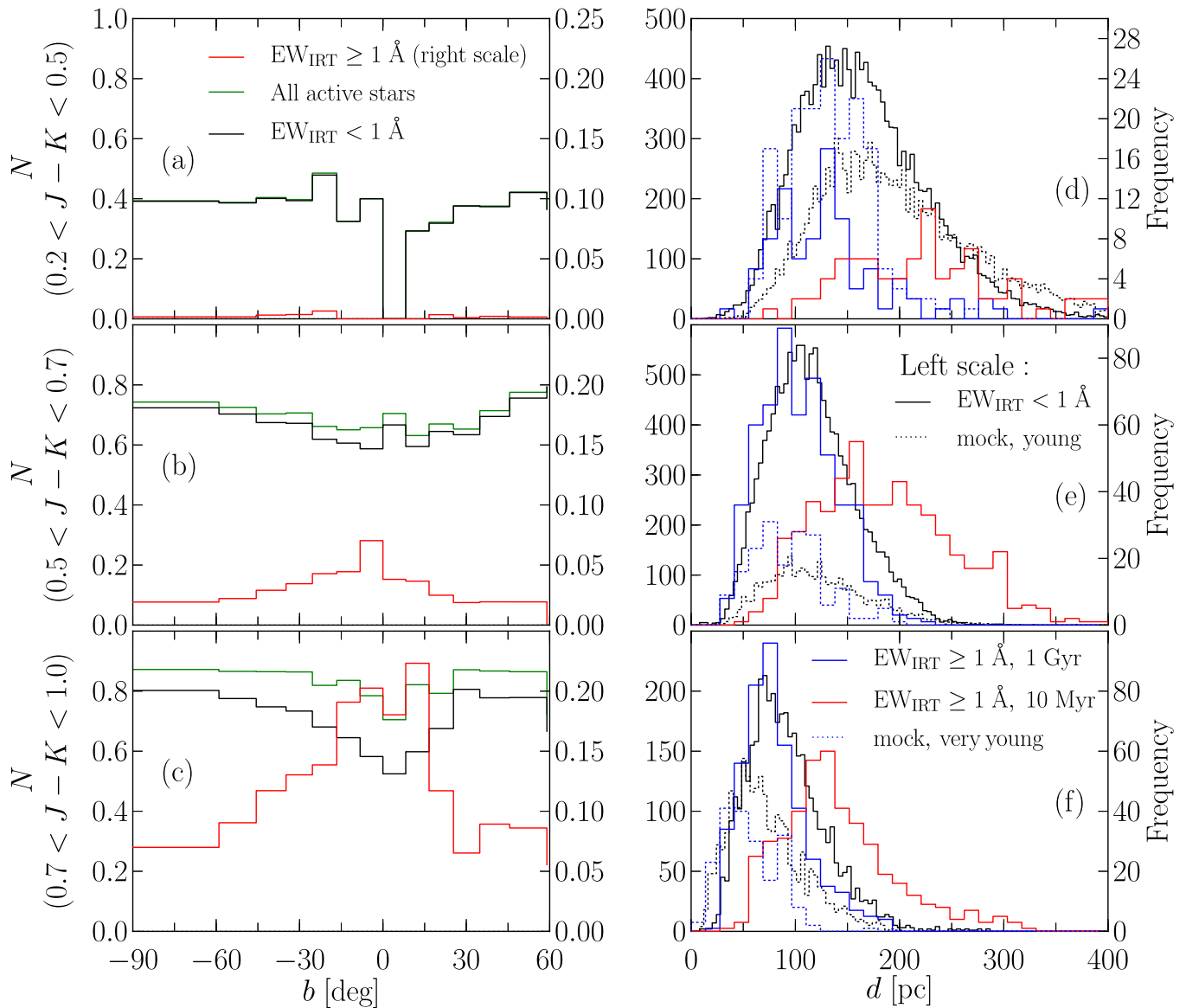


Figure 12. Left: number of active stars over the number of all RAVE dwarfs with $\log g > 3.75$ vs. the Galactic latitude for three color classes. Uneven bin sizes correspond to areas with equal surface in the sky. The most active stars (red line; scale on the right) concentrate at low Galactic latitudes. Distributions for all active stars (green line) and stars with $\text{EW}_{\text{IRT}} < 1 \text{ \AA}$ (black line) are given for reference (their scale is on the left). Right: isochronal *heliocentric* distance estimates at 1 Gyr. Because more active stars (especially solar-like ones with $0.2 < J - K < 0.5$, panel (d)) on average have smaller distances than less active stars, an additional 10 Myr distance was determined as an upper limit for this group as it is evident that they might still reside in their pre-main-sequence phases. Histograms for stars with $\text{EW}_{\text{IRT}} < 1 \text{ \AA}$ (solid and dotted black line) are shown according to the left axis while the scale for stars with $\text{EW}_{\text{IRT}} \geq 1 \text{ \AA}$ (solid and dotted blue and red line) is shown on the right. Distribution of mock-RAVE stars (using the Galaxia model) is shown for comparison (dashed lines; “young stars” mark sample of objects with ages corresponding to $0.1 \text{ \AA} < \text{EW}_{\text{IRT}} < 1 \text{ \AA}$, “very young stars” would show $\text{EW}_{\text{IRT}} > 1 \text{ \AA}$ at their age).

appear to be extremely young, probably still on their way to the main sequence. Again, the correlation between the activity and color of the coolest stars questions the nature of magnetic fields affected by stellar mass and the structure of convective envelopes.

In order to further investigate the young age of the sample, a study of the age– EW_{IRT} relation and its calibration is presented as the main result of this paper (Section 4). A clear correlation between external catalog ages and EW_{IRT} (Figure 10) enabled a coarse calibration of the relation on a large scale (Equation (2)) because on smaller scales the scatter is significant. We introduce three age classes (above 1 Gyr, between 1 Gyr and 100 Myr, and younger than 100 Myr) based on the stellar emission levels. Despite the large uncertainties, the EW_{IRT}

obtained from a single spectroscopic observation of a mid-range resolving power enables the identification of extremely young stars. The latter are of special interest for the establishment of candidate catalogs in the large surveys and further detailed study due to the possibility that they host exoplanets in young stages aside from recent star formation history. Figure 13 presents the probability for the activity rate for a randomly observed dwarf in the solar neighborhood with known $J - K$ color. At $J - K > 0.8$, more than 60% of the stars show signs of activity detectable in RAVE, and almost 10% of the stars have $\text{EW}_{\text{IRT}} > 1 \text{ \AA}$ (i.e., are younger than 100 Myr).

Solar-like stars settle on the main sequence sooner and evolve faster than very red dwarfs, which makes the age–activity relation color dependent. The population of the most

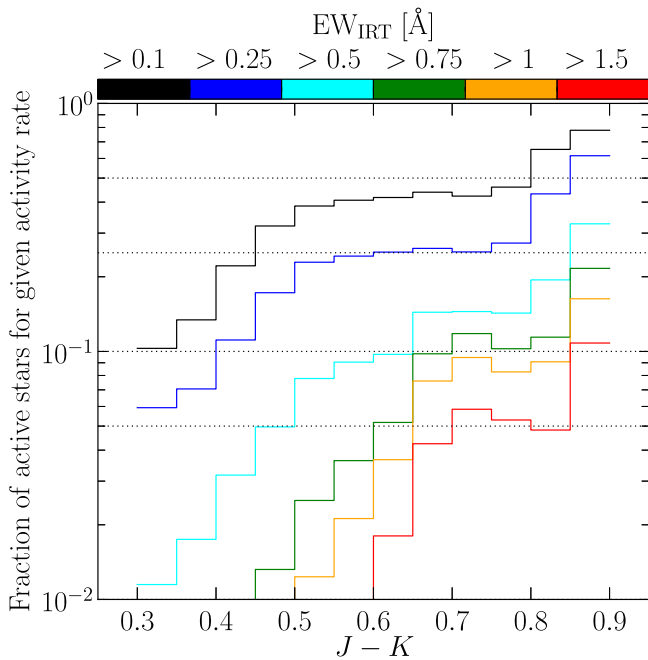


Figure 13. Probability for any detectable signs of activity present in the RAVE’s Ca II IRT above a selected EW_{IRT} threshold for a randomly observed dwarf with known $J - K$ in the solar neighborhood within ~ 300 pc. The ratio of the number of active stars above the selected activity rate over the number of all RAVE dwarf stars is shown for each color bin. Dotted horizontal lines mark the 5%, 10%, 25%, and 50% levels.

active RAVE stars confirms the theory as solar-like stars with $EW_{\text{IRT}} > 0.75 \text{ \AA}$ younger than 100 Myr already reached the main sequence (Figure 7). The color dependence of the relation is not taken into account in this work because no trend is evident in the data.

The distribution of ages for all candidate active RAVE stars is shown in Table 5. About 14,000 stars (11% of all RAVE dwarfs) are estimated to be younger than 1 Gyr and ~ 2000 (1.6%) younger than 100 Myr. The majority of the youngest stars are very red ($J - K > 0.5$) and probably lies off the main sequence, while stars younger than 1 Gyr tend to be hotter, as expected from Figures 7 and 13. The fraction of the coolest stars younger than 100 Myr (0.125) in the RAVE sample is ~ 3 times higher than the fraction in the mock-RAVE catalog (0.038). The sample is a tracer of (a) recent large-scale star formation event(s) that occurred in the solar neighborhood in the southern Galactic hemisphere, possibly due to the crossing(s) of the spiral arm(s). Zuckerman & Song (2004, p. 710 and references therein) claim that a connection between nearby, young stellar groups and Scorpius–Centauri region (the nearest site of massive star formation) is evident and that, “unless the Scorpius–Centauri mass function is very different from those of other star-forming regions, there must have been a handful of supernova explosions that triggered and later dispersed the maternal clouds of the young nearby groups.” An analysis with Gaussian mixture models done by Bovy et al. (2009) on Galactocentric velocities of nearby *Hipparcos* stars (with distances less than 100 pc) revealed that a large fraction of nearby stars (about 40%) live their lives in a small number of moving groups. Murgas et al. (2013) analyzed a sample of ~ 1000 stars from several catalogs of active stars (both Ca II H&K and ultraviolet data) that have kinematic data available. They showed that areas with higher density and

Table 5
Color-dependent Distribution of the Youngest RAVE Stars Over the Age Classes

$J - K$	Age < 1 Gyr $N (N/N_{\text{RAVE}})$	Age < 100 Myr $N (N/N_{\text{RAVE}})$
0.2–0.5	5274 (0.055)	216 (0.002)
0.5–0.7	6135 (0.233)	811 (0.031)
0.7–0.9	3203 (0.431)	932 (0.125)
Total	14,612 (0.113)	1959 (0.016)

Note. The ratio of the number of active stars (N) over the number of all RAVE dwarfs (N_{RAVE}) in a particular bin (130,000 altogether) is presented in the brackets. Note that the total amount of active stars (the bottom line) is slightly larger than the sum of the color-dependent numbers because not all stars have 2MASS photometry available.

activity higher than average in the $U - V$ velocity plane correlate with the known positions of moving groups and clusters. Antoja et al. (2012) detected significant overdensities in the velocity distributions of the RAVE disk stars in and beyond the solar neighborhood (they report on the main local kinematic groups to be large-scale features surviving at least up to ~ 1 kpc from the Sun). According to their findings, a large number of young RAVE stars probably belong to known (or possibly still undiscovered) moving groups and recently disrupted clusters. Orbital simulations would provide more detailed insight into this matter. Their photometric distances remain unreliable (Section 5), but around 50% of the sample is found in the TGAS catalog. Since the database consists of dwarfs in the solar neighborhood, their parallaxes and proper motions are expected to be derived with high accuracy and precision. Distances will enable the accurate placement of objects on the isochrones. The RAVE sample of young active stars thus represents a valuable data set to study not only the recent star formation history but the stellar physics of young and cool objects as well.

Funding for RAVE has been provided by the Anglo-Australian Observatory; the Leibniz-Institut fuer Astrophysik Potsdam; the Australian National University; the Australian Research Council; the French National Research Agency; the German Research foundation; the Istituto Nazionale di Astrofisica at Padova; The Johns Hopkins University; the National Science Foundation of the USA (AST-0908326); the W.M. Keck foundation; the Macquarie University; the Netherlands Research School for Astronomy; the Natural Sciences and Engineering Research Council of Canada; the Slovenian Research Agency; Center of Excellence Space.si; the Swiss National Science Foundation; the Science & Technology Facilities Council of the UK; Opticon; Strasbourg Observatory; and the Universities of Groningen, Heidelberg, and Sydney. The RAVE web site is at <http://www.rave-survey.org>.

This research made use of the cross-match service, the SIMBAD database and the VizieR catalog access tool provided by CDS, Strasbourg.

This publication makes use of data products from the Two Micron All Sky Survey, which is a joint project of the University of Massachusetts and the Infrared Processing and Analysis Center/California Institute of Technology, funded by the National Aeronautics and Space Administration and the National Science Foundation.

Table 6
Table of 137 Stars with Known Ages from the Literature

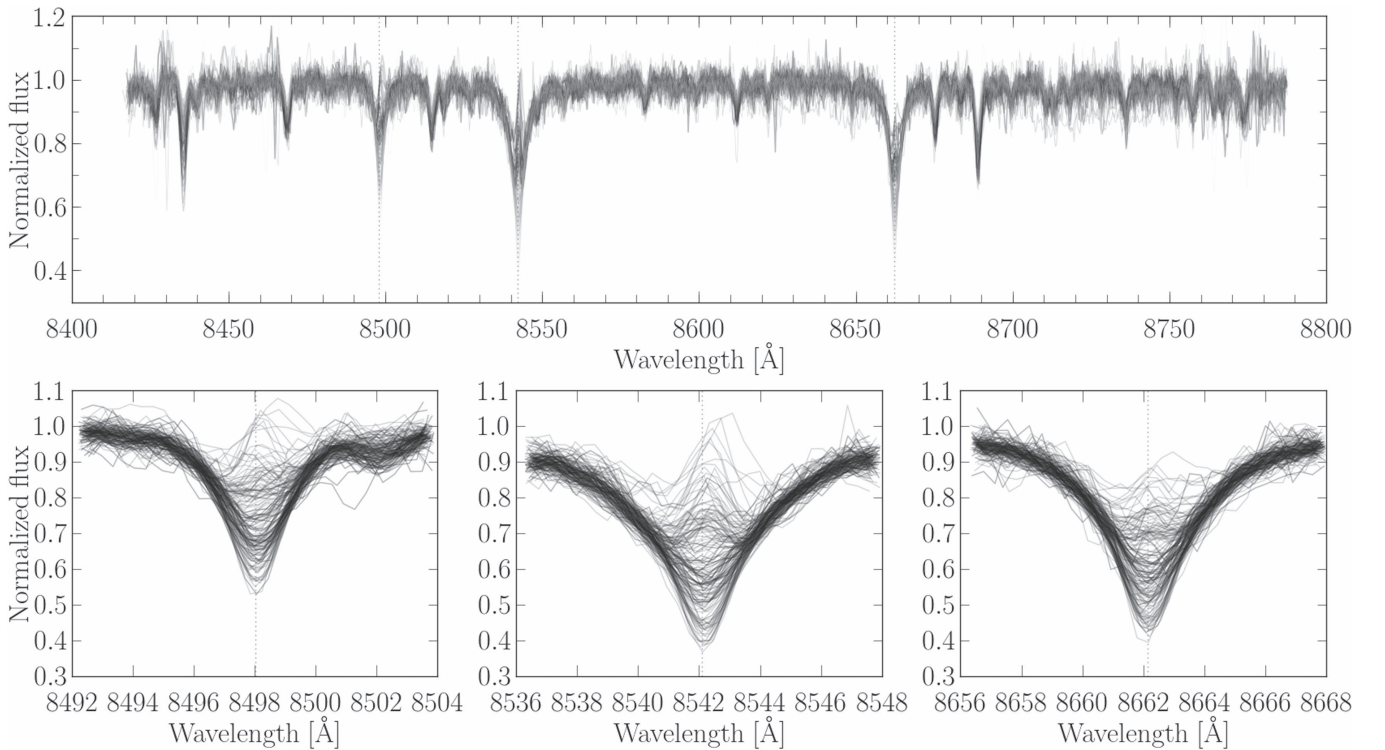
R.A. (deg)	Decl. (deg)	S/N	EW_{IRT} (Å)	Age (Myr)	Group/log R'_{HK}	$N_{\text{UV}} - V$ (mag)	$B - V$ (mag)	$J - K$ (mag)	$W_1 - W_2$ (mag)	Sp. Type	Simbad Type
240.84862	-17.86169	29	1.69	0.4 ^M	Sco Cen Upper	...	1.58	1.02	0.090	M2	PMS, X, IR
239.75871	-18.73725	35	1.82	0.7 ^M	Sco Cen Upper	...	1.28	0.90	0.057	K7	PMS, T Tau, X, IR
235.27850	-26.94056	64	1.60	3 ^M	Sco Cen Upper	...	0.89	0.59	-0.021	K1V	PMS, X, IR
240.16913	-22.00886	44	2.16	4 ^M	Sco Cen Upper	...	0.98	0.64	-0.019	G9	X, PMS, T Tau, IR
226.48692	-43.20089	28	1.48	5 ^M	Lupus	0.85	-0.002	K7	Y, T Tau, IR, X, Star
62.98200	-58.02986	35	0.78	8 ^T	Octans	4.7	0.19	0.43	-0.037	G6V	PMS, Var, IR, X
89.54925	-35.01375	46	1.24	8 ^T	Octans	...	0.69	0.45	-0.035	G9V	X, PMS, Var, IR
168.35929	-45.39522	67	2.50	8 ^T	TW Hya	0.92	0.108	M0.5	T Tau, Var, IR, X
170.27292	-38.75453	34	2.08	8 ^T	TW Hya	6.6	1.45	0.95	0.096	M1Ve	T Tau, Var, IR, X, Star
296.76612	-78.96197	20	1.39	8 ^T	Octans	...	0.79	0.53	-0.004	G8V	PMS, Var, IR, X
179.92613	-76.02392	22	1.16	9 ^T	Eta Cha	7.3	1.13	0.84	-0.035	K4Ve	T Tau, X, Var, IR
189.83850	-75.04422	61	1.62	9 ^T	Eta Cha	...	0.98	0.66	-0.026	K3Ve	T Tau, X, Var, IR
194.60667	-70.48031	125	1.98	9 ^T	Eta Cha	...	0.82	0.64	-0.038	K0Ve	PMS, X, Var, IR
200.53137	-69.63672	25	3.24	9 ^T	Eta Cha	0.98	0.394	K1Ve	Em, PMS, T Tau, Var, IR, X, Star
75.19646	-57.25711	56	1.65	10 ^T	Beta Pic	7.3	1.19	0.85	0.036	M0Ve	PMS, Var, IR, X
175.36513	-73.78417	24	1.38	10 ^T	Cha-Near	...	0.76	0.53	-0.019	G5	IR
281.71900	-62.17686	64	1.80	10 ^T	Beta Pic	...	1.44	0.89	0.043	M1Ve	Var, IR, X, PMS
320.20812	-53.03417	56	1.34	10 ^W	Tuc/Hor	0.48	-0.057	G7V	PMS, Var, IR, UV, X
10.58471	-77.79436	92	1.49	30 ^T	Tuc/Hor	...	0.99	0.69	-0.028	K3Ve	PMS, Var, IR, X
28.06092	-52.32589	26	1.53	30 ^T	Columba	6.5	0.88	0.65	-0.041	K2V(e)	Var, IR, X, PMS
39.21542	-52.05103	92	2.20	30 ^T	Tuc/Hor	...	1.42	0.92	0.103	M2Ve	Var, X, Fl, IR
40.63750	-57.66017	88	1.63	30 ^T	Tuc/Hor	...	1.19	0.78	-0.024	K5Ve	Var, X, PMS, IR
52.70458	-45.93261	112	1.43	30 ^T	Tuc/Hor	...	1.01	0.67	-0.028	K3V	X, PMS, Var, IR
52.98183	-43.98711	59	1.72	30 ^T	Tuc/Hor	7.4	1.22	0.83	0.008	K6Ve	PMS, Var, IR, X
63.59404	-38.31714	79	0.91	30 ^T	Columba	4.8	0.93	0.32	-0.023	G3V	PMS, Var, IR, X
65.29304	-24.53919	73	1.32	30 ^T	Columba	0.40	-0.023	G2V	PMS, Var, IR, X
72.97312	-46.78706	84	1.20	30 ^T	Columba	5.1	0.58	0.38	-0.004	G5V	PMS, Var, IR, X
73.20633	-19.91711	69	1.48	30 ^T	Tuc/Hor	6.5	0.88	0.72	-0.037	...	Var, IR, X
74.64904	-15.62517	33	1.45	30 ^T	Columba	...	0.78	0.46	-0.133	...	IR
74.70217	-8.72772	25	1.68	30 ^T	Columba	...	0.71	0.51	-0.033	...	IR, X
74.88346	-19.29489	68	1.33	30 ^T	Tuc/Hor	...	1.04	0.70	-0.060	...	Var
75.21608	-41.01850	94	1.23	30 ^T	Columba	0.38	-0.031	G5V	IR, X, PMS
85.64267	-34.26172	33	1.45	30 ^T	Tuc/Hor	...	0.82	0.54	-0.042	...	Star
86.31767	-38.61364	59	1.51	30 ^T	Columba	...	0.75	0.48	-0.025	G9V	Var, IR, X
96.52879	-41.04828	101	1.16	30 ^T	Columba	5.8	0.68	0.51	-0.037	K0V	PMS, Var, IR, X
97.02533	-48.44797	75	1.56	30 ^T	Columba	...	0.77	0.53	-0.046	G9V	Var, X, PMS, IR
110.34879	-57.34361	55	1.37	30 ^T	Carina	5.8	0.72	0.51	-0.019	K0V	Var, X, PMS, IR
132.52254	-75.91058	54	1.40	30 ^T	Carina	...	0.70	0.55	-0.049	G9V	T Tau, Var, X, IR
326.12550	-60.97750	66	1.94	30 ^T	Tuc/Hor	7.2	1.35	0.88	0.026	M0Ve	PMS, Var, IR, X
351.54454	-73.39719	37	1.83	30 ^T	Tuc/Hor	6.9	1.43	0.90	0.058	M0Ve	PMS, Var, IR, X
156.40950	-64.68486	53	0.32	32 ^D	IC 2602 ^{C,D}	...	0.80	0.54	-0.060	...	Star
159.57371	-64.13514	47	0.69	32 ^D	IC 2602 ^{C,D}	0.38	-0.032	G5	Cl, IR, X
159.57371	-64.13514	107	0.68	32 ^D	IC 2602 ^{C,D}	0.38	-0.032	G5	Cl, IR, X
160.00017	-63.25308	58	0.72	32 ^D	IC 2602 ^{C,D}	...	0.68	0.36	-0.040	...	IR, X
160.00017	-63.25308	93	0.73	32 ^D	IC 2602 ^{C,D}	...	0.68	0.36	-0.040	...	IR, X
116.85821	-49.04753	50	0.86	40 ^T	Argus	...	0.68	0.50	-0.036	G7V	PMS, Var, IR
117.20762	-43.45156	66	1.94	40 ^T	Argus	...	1.02	0.73	0.006	K4Ve	PMS, Var, IR, X
118.48133	-57.16897	33	1.11	40 ^T	Argus	...	0.81	0.59	-0.032	K0V	X, PMS, Var, IR
128.57567	-52.26603	27	1.27	40 ^T	Argus	...	0.95	0.57	-0.052
128.93204	-53.35564	27	1.70	40 ^T	Argus ^{C,D} , IC 2391 ^{C,D}	...	0.92	0.66	-0.011	...	Star
129.22913	-53.14286	50	1.18	40 ^T	Argus	...	0.80	0.50	-0.056	...	Cl, Var
130.06771	-52.94144	38	1.84	40 ^T	Argus	...	0.72	0.57	-0.018	G9	Cl, Var, X
130.75171	-53.90211	55	1.06	40 ^T	Argus ^{C,D} , IC 2391 ^{C,D}	...	0.69	0.50	-0.005	...	IR
135.51642	-58.14717	50	1.50	40 ^T	Argus	0.54	-0.035	G8V	X, PMS, Var
146.83275	-40.05272	74	1.40	40 ^T	Argus	5.7	0.73	0.53	-0.033	K0V	PMS, IR, X
301.84904	-51.79086	67	1.80	40 ^T	Argus	...	1.23	0.77	-0.028	K6Ve	PMS, Var, IR, X
130.75171	-53.90211	23	0.88	45 ^D	IC 2391 ^{C,D}	...	0.69	0.50	-0.005	...	IR

Table 6
(Continued)

R.A. (deg)	Decl. (deg)	S/N	EW _{IRT} (Å)	Age (Myr)	Group/log R'_{HK}	$N_{UV} - V$ (mag)	$B - V$ (mag)	$J - K$ (mag)	$W_1 - W_2$ (mag)	Sp. Type	Simbad Type
135.12738	-61.57603	60	1.06	60 ^D	Platais 8 ^{C,D}	...	0.59	0.50	-0.021	...	IR
0.79500	-30.18025	46	0.46	62 ^D	Blanco 1 ^{C,D}	0.31	-0.023	...	Cl, IR
1.16329	-32.11753	65	0.18	62 ^D	Blanco 1 ^{C,D}	0.50	-0.058	...	Star
1.51412	-32.15508	62	0.36	62 ^D	Blanco 1 ^{C,D}	6.2	0.81	0.55	-0.051	...	Star
1.64696	-32.80175	38	0.32	62 ^D	Blanco 1 ^{C,D}	4.8	0.62	0.37	-0.019	...	IR
74.34304	-9.13317	75	1.28	70 ^T	AB Dor	5.2	0.73	0.40	-0.051	G5	IR
75.62679	-39.98694	39	1.31	70 ^T	AB Dor	7.1	1.04	0.68	-0.046	K4V	X, PMS, Var, IR
76.61533	-15.82506	104	0.63	70 ^T	AB Dor	...	0.53	0.29	-0.034	F8V	Var, IR, X
90.59129	-13.92569	59	1.03	70 ^T	AB Dor	...	1.07	0.67	-0.043	...	IR, X
92.14108	-34.04861	37	1.44	70 ^T	AB Dor	...	0.75	0.52	-0.017	G9Ve	PMS, Var, IR, X
100.32708	-38.34333	59	2.25	70 ^T	AB Dor	...	0.92	0.66	-0.019	K2Ve	PMS, Var, IR, X
101.97237	-57.22556	29	0.98	70 ^T	AB Dor	7.3	0.99	0.75	-0.048	K4V	Var, X, IR
112.74804	-84.32433	71	1.33	70 ^T	AB Dor	...	0.51	0.50	-0.025	G9V	PMS, Var, IR, X
151.85475	-46.36378	36	0.95	70 ^T	AB Dor	...	1.09	0.70	-0.064	K4V	PMS, IR, X
287.74096	-60.27228	124	0.66	70 ^T	AB Dor	0.32	-0.013	G1V	PMS, Var, IR, X
318.27200	-17.48686	49	1.11	70 ^T	AB Dor	7.5	1.16	0.77	-0.075	K6Ve	PMS, Var, IR, X
53.50754	24.88089	53	0.54	135 ^D	Pleiades ^C	5.4	0.71	0.40	-0.046	...	Cl, IR
53.88204	22.82358	71	0.22	135 ^D	Pleiades ^C	0.29	-0.051	...	Cl, IR
54.59408	22.49969	68	0.55	135 ^D	Pleiades ^C	...	0.56	0.32	-0.050	F8	Cl, IR
54.73696	24.56981	59	0.44	135 ^D	Pleiades ^C	...	0.60	0.32	-0.043	...	Cl, IR
54.80617	24.46653	65	0.54	135 ^D	Pleiades ^{C,D}	...	0.60	0.33	-0.021	...	Cl, IR
54.86583	23.89500	41	0.66	135 ^D	Pleiades ^C	...	0.85	0.48	-0.057	...	Cl
54.92158	23.29089	72	0.43	135 ^D	Pleiades ^{C,D}	...	0.45	0.29	-0.028	G	Cl, IR
55.12804	24.48731	27	0.83	135 ^D	Pleiades ^C	...	0.86	0.53	-0.017	...	Cl, IR
55.14317	23.68261	53	0.71	135 ^D	Pleiades ^C	...	0.73	0.44	-0.043	...	Cl, IR
55.36592	23.70836	49	0.84	135 ^D	Pleiades ^C	...	0.75	0.45	-0.062	...	Cl
55.40067	25.61931	80	0.48	135 ^D	Pleiades ^{C,D}	...	0.58	0.37	-0.021	...	Cl, IR
56.72400	23.58356	52	0.44	135 ^D	Pleiades ^C	...	0.57	0.35	-0.047	G0V	Cl, IR
56.72400	23.58356	78	0.51	135 ^D	Pleiades ^C	...	0.57	0.35	-0.047	G0V	Cl, IR
57.35717	24.93764	33	0.74	135 ^D	Pleiades ^{C,D}	...	0.87	0.48	-0.057	G2	Cl, IR, X
57.35717	24.93764	23	0.90	135 ^D	Pleiades ^C	...	0.87	0.48	-0.057	G2	Cl, IR, X
57.58875	23.09639	26	0.48	135 ^D	Pleiades ^C	...	0.91	0.48	-0.065	...	Cl, IR
57.58875	23.09639	57	0.49	135 ^D	Pleiades ^C	...	0.91	0.48	-0.065	...	Cl, IR
57.92533	21.66836	38	0.63	135 ^D	Pleiades ^C	...	0.83	0.45	-0.067	...	Cl
58.00933	24.66331	20	2.09	135 ^D	Pleiades ^C	...	1.07	0.73	0.008	K3V	Cl, Em, T Tau, Var, Fl, IR, X
327.59629	-16.19647	132	0.47	150 ^I	-4.33	...	0.65	0.40	-0.073	G7V	IR
209.06946	-62.35256	30	0.20	169 ^D	Platais 12 ^{C,D}	...	0.60	0.34	-0.041	...	IR
65.88471	14.67047	93	0.67	380 ^I	Hyades	...	0.73	0.47	-0.034	G5	Cl, X, IR
67.49054	16.67283	131	0.56	400 ^I	Hyades	6.6	0.79	0.48	-0.062	K1V	Cl, X, IR
0.16796	-69.67597	121	0.72	512 ^A	-4.47	6.6	0.87	0.55	-0.033	K1V	IR
50.58333	-36.63717	72	1.28	524 ^K	Alessi 13 ^C	5.0	0.73	0.41	-0.039	G5	IR
53.08567	-38.74736	23	0.05	524 ^K	Alessi 13 ^C	6.2	0.74	0.47	-0.059	...	IR
67.01850	13.86794	55	0.64	630 ^I	Hyades	...	0.72	0.50	-0.034	G5	Cl, IR
66.05325	16.37892	67	0.22	787 ^D	Hyades	...	0.56	0.28	-0.021	G0V	Cl, X, IR
66.85558	14.26067	83	0.70	787 ^D	Hyades	...	1.04	0.66	-0.051	K2	Cl, IR
66.94600	14.41775	46	0.51	787 ^D	Hyades	...	0.70	0.55	-0.040	K0	Cl, X, IR
67.04529	16.47094	79	0.03	787 ^D	Hyades	...	1.37	0.80	-0.068	K5	Cl, IR
68.40817	16.76250	99	0.71	787 ^D	Hyades	6.8	0.87	0.49	-0.042	G5	Cl, hPM, X, IR
68.63408	15.82756	116	0.68	787 ^D	Hyades	...	0.80	0.51	-0.057	K0	Cl, IR
71.89725	14.88908	48	0.30	787 ^D	Hyades	8.4	1.34	0.74	-0.067	M0V	Cl, Var
72.21533	15.94756	68	0.78	787 ^D	Hyades	0.50	-0.060	...	IR
72.50296	16.41206	76	0.02	787 ^D	Hyades	...	1.10	0.65	-0.080	K0	Cl, IR
72.95496	17.27372	37	0.37	787 ^D	Hyades	0.74	-0.079	K5	hPM
74.25283	13.91236	104	0.23	787 ^D	Hyades	...	1.13	0.64	-0.092	...	Cl
75.40696	12.41639	53	0.36	787 ^D	Hyades	8.1	1.34	0.85	0.013	...	Star
39.03250	-28.21833	82	-0.00	880 ^I	-4.67	...	0.76	0.43	-0.067	G9V	IR
74.45629	14.00219	61	0.48	970 ^I	Hyades	-4.57	0.65	0.33	-0.076	G5	Cl, IR
69.73879	14.10558	119	0.40	350 ^I , 1122 ^W	Hyades	0.37	-0.046	G5	Cl, IR
47.17717	-35.43289	213	-0.02	1220 ^I	-4.61	5.7	0.56	0.41	0.213	G3V	IR
244.22125	-49.85675	114	0.33	1230 ^A	-4.67	0.45	-0.032	G8IV-V	IR
277.82900	-18.90881	133	0.36	1260 ^I , 1621 ^W	-4.71, -4.65	0.58	0.350	K2V	Cl, hPM, Var, IR
36.86792	-27.63500	41	0.06	1940 ^I	-4.70	0.51	-0.062	K1V	hPM, IR

Table 6
(Continued)

R.A. (deg)	Decl. (deg)	S/N	EW _{IRT} (Å)	Age (Myr)	Group/log R'_{HK}	$N_{UV} - V$ (mag)	$B - V$ (mag)	$J - K$ (mag)	$W_1 - W_2$ (mag)	Sp. Type	Simbad Type
5.64492	-73.03236	123	0.17	2290 ^A	-4.73	...	0.70	0.41	-0.060	G8V	IR
17.24133	-30.92925	71	0.15	2570 ^A	-4.75	0.47	-0.073	G8/K0V	hPM, IR
25.65417	-58.41317	150	-0.00	3019 ^A	-4.79	...	0.79	0.42	-0.034	G6V	IR
30.19675	-80.53269	36	0.09	3548 ^A	-4.82	0.45	-0.047	K1V	IR
279.72250	-21.05186	238	0.08	5360 ^I , 3890 ^W	-4.93, -4.90	0.56	0.352	G6V	IR, UV
1.24463	-70.21244	82	0.10	4073 ^A	-4.88	5.8	0.66	0.38	-0.036	G5V	IR
180.18521	-10.44603	184	0.22	7350 ^I , 4168 ^W	-4.89, -4.92	0.53	...	G8IV	hPM, IR, UV
183.46604	-69.06050	119	0.03	5370 ^A	-4.97	0.56	-0.040	K2V	hPM, IR
26.90958	-26.75000	45	-0.06	6860 ^I , 5495 ^W	-5.04, -5.00	0.50	-0.061	G9V	hPM, IR
168.00483	-26.13664	123	0.17	7470 ^I , 5495 ^W	-5.01, -5.00	0.48	0.163	G8.5V	hPM, IR
193.84079	-4.50417	185	0.03	5940 ^I	-4.97	6.5	0.70	0.46	0.127	G5	hPM, IR
260.71371	-2.38817	237	-0.08	5810 ^I , 6309 ^W	-5.03, -5.04	0.45	0.436	G5IV	IR, UV
265.93437	-3.91786	154	0.03	6456 ^A	-4.99	0.40	0.024	G5	hPM, IR
32.53333	-31.06972	38	0.09	6918 ^A	-5.02	0.42	-0.085	K0V	hPM, IR
209.11283	-16.19622	78	-0.14	7000 ^I	-5.02	0.44	-0.071	G9V	hPM, IR
189.02742	-42.85231	31	0.45	8128 ^A	-5.00	0.37	-0.022	G5V	IR
318.36537	-49.79458	120	0.07	9120 ^A	-5.15	...	0.52	0.41	-0.054	G6IV	IR
16.99858	1.99306	111	-0.16	10964 ^W	-4.92	0.60	0.345	K0IV	hPM, IR

**Figure 14.** Normalized RAVE fluxes of 137 active spectra used in the age–activity calibration. Their parameters together with age are listed in the Table 6. Calcium lines are shown separately in the bottom panels.

APPENDIX REFERENCE STELLAR AGES

One hundred and thirty seven active RAVE spectra were used for the calibration of the age–activity relation. A small portion of spectra are repeated measurements of the same object. Such cases are treated independently in the age–activity relation calibration procedure. Table 6 lists all active RAVE candidates where external ages are available in the literature.

All spectra are depicted in Figure 14 and show adequate behavior, i.e., no peculiarities other than emission in calcium. Their activity levels range from negative values up to ~ 3 Å.

The first two columns of the table list the R.A. and decl. of a star (J2000.0), followed by the signal-to-noise (S/N per pixel) estimation. Only spectra with $S/N > 20$ are included. Equivalent widths of excessive flux EW_{IRT} are a quantitative evaluation of emission levels. The references for cluster or moving group membership are the same as for the age if not

stated otherwise. The references are marked as follows: A (Arriagada 2011), C (Conrad et al. 2014), D (Dias et al. 2012), I (Isaacson & Fischer 2010), K (Kharchenko et al. 2013), M (Makarov 2007), T (Torres et al. 2008), and W (Wright et al. 2004). Where $\log R'_{HK}$ is known, ages in the original papers were derived from their $\log R'_{HK}$ -age relations. Ages of seven stars were derived by two different teams. We list both values in such cases. Ages for one such star (Hyades member) are estimated to be of different orders of magnitude (and differ from the generally accepted Hyades age) while ages for the rest of them are comparable. Other values rely on the age estimated from known stellar clusters and moving groups (column “Group”; the membership reference is the same as for the age, if not stated otherwise). Two stars were found to be candidate members of two moving groups (Argus and IC 2391) at the same time. The table is supplemented by $N_{UV} - V$, $B - V$, $J - K$, and $W_1 - W_2$ colors. For a discussion on this matter, see Section 3. Additional information is provided by the columns “Sp. Type” and “Simbad Type” marking spectral types and morphological classification available on the online Simbad database. Abbreviations for Simbad types are PMS (Pre-main-sequence star), X (X-ray source), UV (UV-emission source), IR (Infrared source), hPM (High proper-motion Star), Cl (Star in Cluster), Var (Variable Star), Fl (Flare Star), B (Star in double system), Multi (Double or multiple star), Em (Emission-line Star), Y (Young Stellar Object), and sub-mm (sub-millimetric source). This publication makes use of data products from the Wide-field Infrared Survey Explorer, which is a joint project of the University of California, Los Angeles, and the Jet Propulsion Laboratory/California Institute of Technology, funded by the National Aeronautics and Space Administration.

REFERENCES

- Antoja, T., Helmi, A., Bienayme, O., et al. 2012, *MNRAS*, **426**, L1
- Arriagada, P. 2011, *ApJ*, **734**, 70
- Bailer-Jones, C. A. L., Andrae, R., Arcay, B., et al. 2013, *A&A*, **559**, A74
- Baliunas, S. L., Donahue, R. A., Soon, W. H., et al. 1995, *ApJ*, **438**, 269
- Barnes, S. A. 2007, *ApJ*, **669**, 1167
- Barry, D. C., Cromwell, R. H., & Hege, E. K. 1987, *ApJ*, **315**, 264
- Bianchi, L., Efremova, B., Herald, J., et al. 2011, *MNRAS*, **411**, 2770
- Binney, J., Burnett, B., Kordopatis, G., et al. 2014, *MNRAS*, **437**, 351
- Bovy, J., Hogg, D. W., & Roweis, S. T. 2009, *ApJ*, **700**, 1794
- Bressan, A., Marigo, P., Girardi, L., et al. 2012, *MNRAS*, **427**, 127
- Conrad, C., Scholz, R.-D., Kharchenko, N. V., et al. 2014, *A&A*, **562**, A54
- Cropper, M., & Katz, D. 2011, in EAS Publications Ser. 45, GAIA: At the Frontiers of Astrometry, ed. C. Turon, F. Meynadier, & F. Arenou (Les Ulis: EDP Sciences), 181
- Cutri, R. M., et al. 2014, *yCat*, **2328**, 0
- De Silva, G. M., Freeman, K. C., Bland-Hawthorn, J., et al. 2015, *MNRAS*, **449**, 2604
- Dias, W. S., Alessi, B. S., Moitinho, A., & Lepine, J. R. D. 2012, *A&A*, **389**, 871
- Feigelson, E. D., & Montmerle, T. 1999, *ARA&A*, **37**, 363
- Freeman, K., & Bland-Hawthorn, J. 2002, *ARA&A*, **40**, 487
- Gallet, F., & Bouvier, J. 2013, *A&A*, **556**, A36
- Gray, R. O., Corbally, C. J., Garrison, R. F., et al. 2006, *AJ*, **132**, 161
- Henden, A., & Munari, U. 2014, *CoSka*, **43**, 518
- Henry, T. J., Soderblom, D. R., Donahue, R. A., & Baliunas, S. L. 1996, *AJ*, **111**, 439
- Høg, E., Fabricius, C., Makarov, V. V., et al. 2000, *A&A*, **355**, L27
- Huber, D., Bedding, T. R., Stello, D., et al. 2011, *ApJ*, **743**, 143
- Isaacson, H., & Fischer, D. 2010, *ApJ*, **725**, 875
- Jeffries, R. D. 2014, in EAS Publications Ser. 65, The Ages of Stars, ed. Y. Lebreton, D. Valls-Gabaud, & C. Charbonnel (Les Ulis: EDP Sciences), 289
- Katz, D., Munari, U., Cropper, M., et al. 2004, *MNRAS*, **354**, 1223
- Kharchenko, N. V., Piskunov, A. E., Schilbach, E., Röser, S., & Scholz, R.-D. 2013, *A&A*, **558**, A53
- Kordopatis, G., Gilmore, G., Steinmetz, M., et al. 2013, *AJ*, **146**, 134
- Kunder, A., Kordopatis, G., Steinmetz, M., et al. 2016, arXiv:1609.03210
- Lachaume, R., Dominik, C., Lanz, T., & Habing, H. J. 1999, *A&A*, **348**, 897
- Li, J., Smith, M. C., Zhong, J., et al. 2016, *ApJ*, **823**, 59
- Lyra, W., & Porto de Mello, G. F. 2005, *A&A*, **431**, 329
- Makarov, V. V. 2007, *ApJ*, **658**, 480
- Mamajek, E. E., & Hillenbrand, L. A. 2008, *ApJ*, **687**, 1264
- Matijević, G., Zwitter, T., Bienaymé, O., et al. 2012, *ApJS*, **200**, 14
- Michalik, D., Lindegren, L., & Hobbs, D. 2015, *A&A*, **574**, A115
- Murgas, F., Jenkins, J. S., Rojo, P., Jones, H. R. A., & Pinfield, D. J. 2013, *A&A*, **552**, A27
- Noyes, R. W., Hartmann, L. W., Baliunas, S. L., Duncan, D. K., & Vaughan, A. H. 1984, *ApJ*, **279**, 763
- Pace, G. 2013, *A&A*, **551**, L8
- Radick, R. R., Lockwood, G. W., Skiff, B. A., & Baliunas, S. L. 1998, *ApJS*, **118**, 239
- Rocha-Pinto, H. J., & Maciel, W. J. 1998, *MNRAS*, **298**, 332
- Roweis, S., & Saul, L. K. 2000, *Sci*, **190**, 2323
- Rutten, R. G. M. 1984, *A&A*, **130**, 353
- Schlegel, D. J., Finkbeiner, D. P., & Davis, M. 1998, *ApJ*, **500**, 525
- Schrjver, C. J., Cote, J., Zwaan, C., & Saar, S. H. 1989, *ApJ*, **337**, 964
- Sharma, S., Bland-Hawthorn, J., Johnston, K. V., & Binney, J. 2011, *ApJ*, **730**, 3
- Siebert, A., Williams, M. E. K., Siviero, A., et al. 2011, *AJ*, **141**, 187
- Skrutskie, M. F., Cutri, R. M., Stiening, R., et al. 2006, *AJ*, **131**, 1163
- Skumanich, A. 1972, *ApJ*, **171**, 565
- Smiljanic, R., Korn, A. J., Bergemann, M., et al. 2014, *A&A*, **570**, A122
- Soderblom, D. R. 2010, *ARA&A*, **48**, 581
- Soderblom, D. R., Duncan, D. K., & Johnson, D. R. H. 1991, *ApJ*, **375**, 722
- Steinmetz, M., Zwitter, T., Siebert, A., et al. 2006, *AJ*, **132**, 1645
- Stelzer, B., Marino, A., Micela, G., López-Santiago, J., & Liefke, C. 2013, *MNRAS*, **431**, 2063
- Torres, C. A. O., Quast, G. R., Melo, C. H. F., & Sterzik, M. F. 2008, in Young Nearby Loose Associations, ed. B. Reipurth (San Francisco, CA: ASP), 757
- Vanderplas, J., & Connolly, A. 2009, *AJ*, **138**, 1365
- Vaughan, A. H., Preston, G. W., & Wilson, O. C. 1978, *PASP*, **90**, 267
- Voges, W., Aschenbach, B., Boller, T., et al. 1999, *A&A*, **349**, 389
- West, A. A., Hawley, S. L., Bochanski, J. J., et al. 2008, *AJ*, **135**, 785
- Williams, M. E. K., Steinmetz, M., Sharma, S., et al. 2011, *ApJ*, **728**, 102
- Wilson, O. C. 1976, *ApJ*, **205**, 823
- Wojno, J., Kordopatis, G., Piffl, T., et al. 2016, arXiv:1611.00733
- Wright, J. T., Marcy, G. W., Butler, R. P., & Vogt, S. S. 2004, *ApJS*, **152**, 261
- Žerjal, M., Zwitter, T., Matijević, G., et al. 2013, *ApJ*, **776**, 127
- Zhao, J.-K., Oswalt, T. D., Chen, Y.-Q., et al. 2015, *RAA*, **15**, 1282
- Zhao, J. K., Oswalt, T. D., Rudkin, M., Zhao, G., & Chen, Y. Q. 2011, *AJ*, **141**, 107
- Zuckerman, B. 2001, *ARA&A*, **39**, 549
- Zuckerman, B., & Song, I. 2004, *ARA&A*, **42**, 685
- Zwitter, T., Siebert, A., Munari, U., et al. 2008, *AJ*, **136**, 421